ABSTRACT

Title of Document: CONSTITUTIVE PROPERTY TESTING AND RELIABILITY ASSESSMENT OF LEAD-FREE SOLDER JOINT

Yuri Lee, Master, 2010

Directed By: Professor Bongtae Han,
Department of Mechanical Engineering

A modified single lap shear test configuration, based on the Iosipescu geometry, is proposed to characterize mechanical properties of solder alloys. In the method, an auxiliary device (extension unit) is employed to improve the accuracy of measurement. The extension unit is attached directly to the test area. The unit converts shear displacements to axial displacements, which are subsequently captured by a high-resolution extensometer. The extension unit allowed measurement of shear deformations without compensating machine and grip compliance.

The proposed test configuration is utilized to characterize the constitutive properties of lead-free solder. Experimental parameters are obtained for (1) a partitioned model, where the elastic, rate-independent plastic and rate-dependent creep behaviors are all separated and (2) a unified creep-plastic model.

Reliability assessment of lead-free solder joint is performed by calibration of virtual qualification model for leaded packages with lead-free solder.

CONSTITUTIVE PROPERTY TESTING AND RELIABILITY ASSESSMENT OF LEAD-FREE SOLDER JOINT

By

Yuri Lee

Thesis submitted to the Faculty of the Graduate School of the
University of Maryland, College Park, in partial fulfillment
of the requirements for the degree of
Master of Science
2010

Advisory Committee:
Professor Bongtae Han, Chair
Professor Abhijit Dasgupta
Dr. Michael Osterman

Table of Contents

List of Tables

List of Figures

Chapter 1: Motivation and Objective

1.1 Motivation

Thermal loading in electronic assemblies causes thermo-mechanical deformation which results in fatigue damage in solder interconnections. Accurate stress analysis of solder interconnections is critical to predict reliability of interconnections, furthermore to optimize design to enhance interconnection reliability. The constitutive properties are one of the most critical parameters for accurate stress analysis. Many researchers conducted experiments to obtain constitutive properties of Tin-Lead eutectic solder including Darveaux, Wang and Ye[1-5]. Yet these published data shows huge variation.

D. Pollack conducted FE analysis using a commercial package (Ansys) for simple geometry under themo-mechanical load. She then compared the results of FE analysis for three different sets of constitutive properties for eutectic solder. [6]

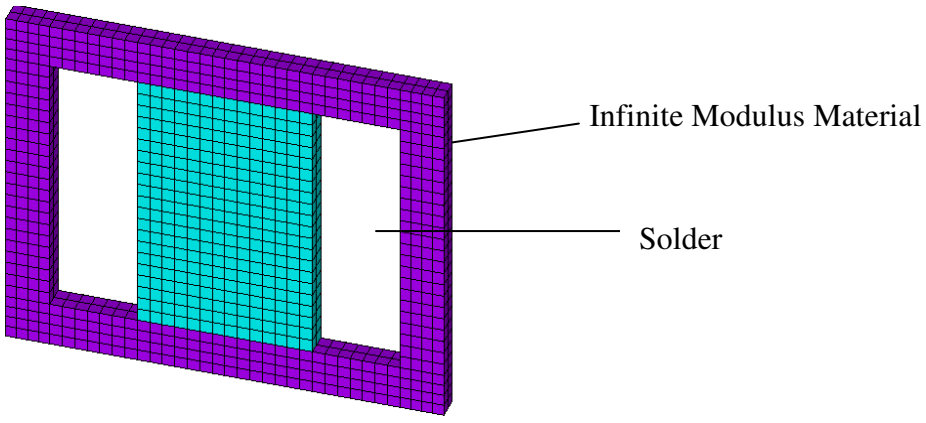

Figure 1 D. Pollack's thermal Coefficient Mismatch Model

The geometry is made of two different materials. Outside frame with infinite modulus and inner solder block with eutectic solder material. When this simple geometry goes under thermal loading from 25 ºC to 125 ºC then dwell at 125 ºC for 10 minutes, the frame will produce tension on the solder. By using two different CTE values as material properties for outside frame, D. Pollack mimicked two different strain rates on solder block. CTE value 30 ppm/ºC produced strain rate magnitude of 10^{-6}/s and CTE value 520 ppm/ºC produced yields strains on the order of a few percent and strain rate magnitude of 10^{4}/s. In both low strain rate and high strain rate test, Properties from Ye showed quite different results than those from Darveaux and Wang. Darveaux's and Wang's showed similar behavior in strain wise but their behaviors were significantly different in stress wise.

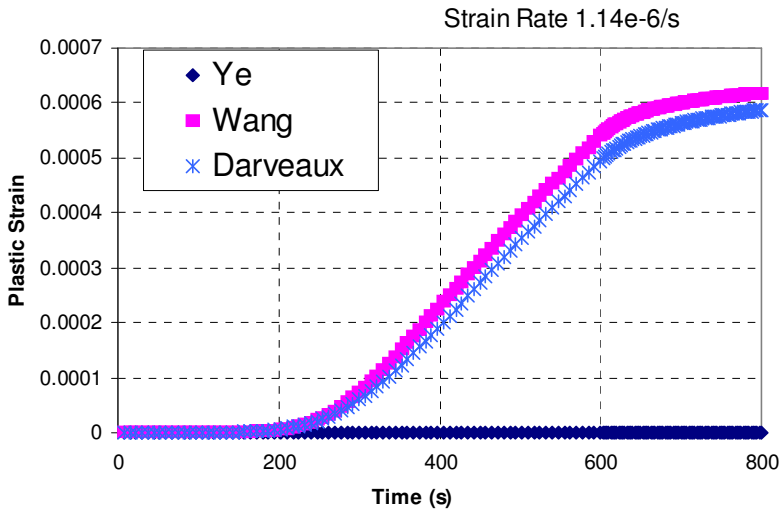

Figure 2 Plastic Strain vs. Time for low strain rate test

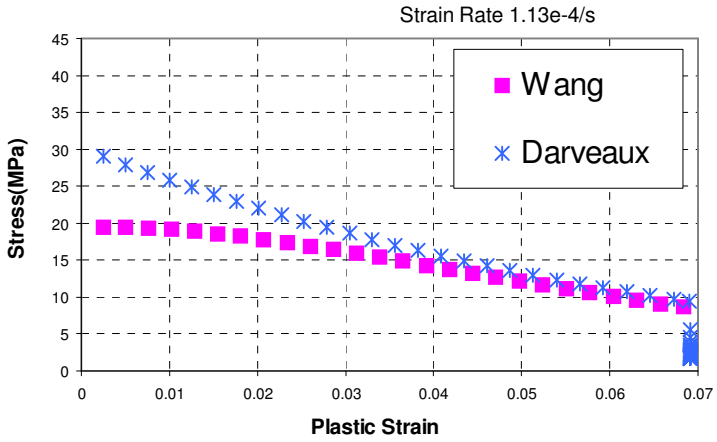

Figure 3 stress vs strain for lower strain rate test

This result verifies why constitutive properties are so critical to accurate stress analysis and motivated us to design experiments to obtain reliable constitutive properties for lead-free solders whose properties were still not available at the time of experiment.

1.2 Objective

The objective of this thesis is to develop an experimental scheme to document the pseudo-continuum behavior of micro scale polycrystalline metals subjected to isothermal mechanical loadings, and to implement the scheme to determine constitutive relationships of a binary lead-free solder (Sn3.5Ag) in electronic package. The obtained constitutive properties through the process can be used for more accurate stress analysis.

1.3 Organization of Thesis

Chapter 2 explains the proposed experimental methodology to measure constitutive properties of solder alloys used in interconnections in electronic packages. This chapter includes the background, the specimen configuration chosen in the proposed test scheme, reason for the specific configuration, test apparatus, grip and specimen configurations.

Chapter 3 is about details in the experiments measuring constitutive properties of Sn3.5Ag solder. It presents specimen preparation procedure, test procedure and actual experimental results. The results of modulus test and constant strain rate tests at different temperatures are presented.

Most parts in chapter 2 and 3 have been published as "Micro Single Lap Shear Test with Direct Local Measurement Scheme" in the proceedings of SEM'03.

Chapter 4 presents constitutive properties of lead free binary solder Sn3.5Ag explaining detain procedures to get the constants in two different forms of constitutive models. In partitioned model, constants have been calculated for elastic, rate-independent plastic and rate-dependent creep model. As a unified model, constants for Anand model have been calculated from the experiments results presented in chapter 3.

Most parts in chapter 3 and chapter 4 were published in CALCE Consortium Report, October 2002.

Chapter 5 discusses the reliability assessment of lead-free solder joint and calibration of virtual qualification model for leaded packages with lead-free solder.

The calibrated thermal fatigue model is presented to be used in calcePWA and calceFAST for packages with ternary lead-free solder (Sn3.9Ag0.6Cu).

Chapter 6 is about conclusions and contributions.

Appendix A contains matlab codes used to obtain Anand constant.

Chapter 2: Proposed Test Scheme - Advanced Micro Shear Test for Solder Alloy

2.1 Background

In order to decide which test configuration to use, first we have to define what kind of solder constitutive properties we are interested.

One of the options will be micro tensile test as we see in Figure 4, especially if you are interested in intrinsic material properties.

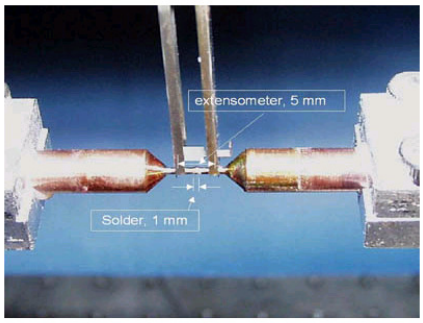

Setup of a uniaxial tensile test on 63Sn-37Pb solder alloy with the Tytror 250.

Figure 4 Picture of micro tensile test (Sandia lab)

Or micro lap shear test can be run as you see in Figure 5.

Figure 5 Micro lap shear test

The constitutive properties of solder we are interested are the one to be used for accurate stress analysis in electronic package. Furthermore that stress analysis will be used to assess damage accumulation due to life-cycle stresses.

In many times solder joints in electronic packaging is under shear force caused by CTE mismatch.as in Figure 6.

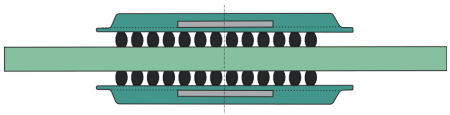

Figure 6 Small solder balls under shear force caused by CTE mismatch

In real application actual solder joints are small and their deformations are constrained by adjacent components by PCB and top and bottom modules in the case of Figure 6. So the grains in solder joints are not completely free to move.

In this study, micro-scale lap shear test is proposed since first it simulates the application boundary condition as in the electronic package; second the constitutive properties obtained from micro lap shear test can represent Pseudo continuum constitutive properties that account for geometrical constraint at the interface.

Stress analysis is based on continuum approach, by using Pseudo continuum constitutive properties we can account for geometrical constrain at the interface.

2.2 Specimen Configuration

The single lap shear test configuration used in the test is illustrated in Figure 7. It is similar to simple notched shear specimen proposed by P. Haswell [7]. It is based on the modified Iosipescu [8] specimen, originally proposed by Reinikainen and Ren [9, 10]. This specimen configuration can be accommodated with a uniaxial tensile

tester. The adherend, fabricated from cold rolled copper, is shown in (a) with relevant dimensions. The solder is sandwiched by the copper plates to complete the specimen assembly as illustrated in (c). The soldered region is 1.5 mm by 2 mm and the solder height is 300μm. The 45° grooves next to the solder joint offer a uniform shear stress along the solder joint while minimizing a stress concentration at the corner in (b) [9]. This configuration hasn't been implemented in measuring constitutive properties before.

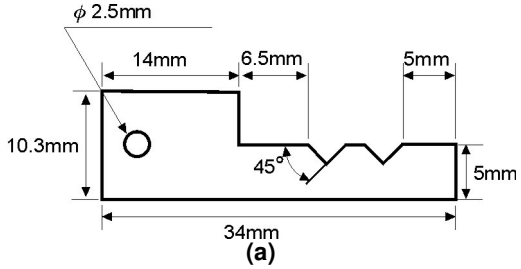

(a)

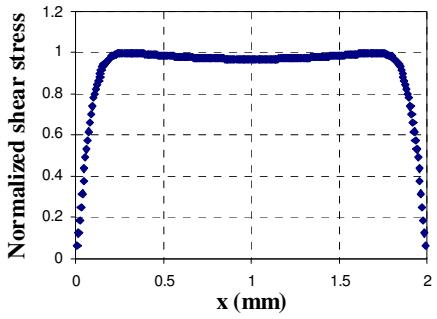

(b)

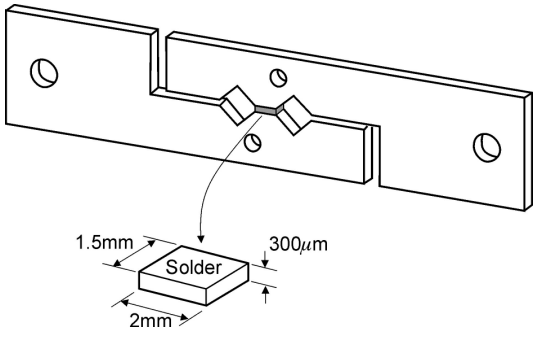

(c)

Figure 7 Geometry of modified micro shear lap specimen.

2.3 Specimen preparation

The proposed modified lab shear solder specimens was produced by conductive manual soldering method as suggested by Zhang [11]. This process ensures minimum void contents and quality. Specimen was produced one at a time using specially designed solder reflow fixture. This fixture helps to position copper strips during reflow process and made precise alignment possible. Steel shim was placed between copper strips to maintain 300μm joint height. The copper strips were fabricated by wiring EDM (Electrical Discharge Machine) to minimized error. Good wetting and precise alignment were two major concerns. The procedure starts with cleaning copper strips. If the oxidation of the joint surface of copper strips is severe, the joint surface was polished minimally and very carefully with fine sand paper (1000A). The polished surface was maintained to be flat for good wetting. Copper strips were cleaned by brushing with Isopropyl alcohol then dipped in flux and placed on hot plate until the flux evaporates. This step was repeated as many times until the copper strips get clean then followed by cleaning with Isopropyl alcohol. Silicone rubber was applied to the surface of the two notches next to the joint surface. The glue prevents the solder from reaching areas on the copper block other than the desired joint surface. 24 hour was allowed for the silicone rubber to dry. Flux was carefully applied on joint surfaces using cotton swab so that applied solder will stick. Copper strips and shim were located in the reflow fixture and fastened with screws in the fixture. A drop of flux was applied to joint surface and the reflow fixture with the copper strips was placed on the 130°C hot plate and wait for 20 seconds. This procedure is to activate the flux. It has to be removed from hot plate before the flux

evaporates. The reflow fixture with the copper strips was placed onto the 250°C hotplate. Finally solder wire dipped in flux was brought to contact the joint surface and filled the gap fully. The specimen was placed on thick aluminum base to cool down.

After soldering and initial inspection, the produced specimen was placed into the specially designed polishing fixture and polished using increasingly fine sandpaper on the grinder then polished polishing powder on the polisher.

The height, width of the solder joint was measured on both sides using optical microscope and the thickness of the joint were measured using screw gauge/micrometer.

2.4 Test Apparatus

MTS Tytron™ 250 Testing System was chosen as a part of test apparatus.

It is uniaxial micro tester for small specimens and its load capacity is up to 250 N and load resolution is 0.001N. The system is composed of hardware and software parts. For the hardware, there are measurement devices, high temperature devices and other accessories like cables and alignment tools etc. Measurement devices are LVDT (Linear Variable Differential Transformer), displacement gage, miniature extensometer and load cells with two different capacities of 10N and 250N. High temperature devices are temperature controller, heat chamber and grips with cooling system. The software is TestStar IIs. It is composed of station manager, station builder, multipurpose testware (MPT) and data acquisition part (A/D converter).

Tytron™ 250 can be controlled either by load or displacement. For displacement control, either LVDT or displacement gage or miniature extensometer can be used.

The test apparatus needed to be tuned for the materials to be tested. Tuning procedure was performed by adjusting PID values for different control modes following the specific order. First was displacement (LVDT) control without specimen, second was load control then displacement control (LVDT) with specimen followed by displacement (extensometer) control with specimen.

The specific tuning values were obtained from the above procedure for different control modes and for different specimens including SnAg, SnAgCu and copper strip.

Figure 8 MTS Tytron™250

To get a high resolution in displacement measurement, a miniature extensometer (MTS 632.29F) was used. It has 3mm gage length. Either 0.8% or 8% of gage length can be chosen for travel length. Since it uses 16bit for communication, resolution of displacement for each travel range can be calculated as follows.

Resolution: $240\mu m / 2^{16} \times 2 = 0.007324\mu m$ (for 8%)

$24\mu m / 2^{16} \times 2 = 0.0007324\mu m$ (for 0.8%)

By dividing the results of the above calculations with the gage length for each travel range, strain resolution can be calculated as follows.

Strain resolution: 0.007324 μm / 3mm = 2.44 μstrain (for 8%)

0.0007324 μm / 3mm = 0.244 μstrain (for 0.8%)

Figure 9 Extensometer picture

The range and resolution of measurement devices are in Table 1.

Table 1 Resolution of Measurement Devices

Measurement Device	Range	Resolution
LVDT	±60mm	1.83 μm
	±5mm	0.153 μm
Displacement Gage	±2mm	0.061 μm
Miniature Extensometer (632.29F-20)	±8% strain	2.44 με (0.0732 μm)
	±0.8% strain	0.244 με (0.00732 μm)
Load cell /Force Transducer	±10N	0.0003 N
	±250N	0.0076 N

2.5 Grip and Specimen Configuration

Also a special grip was designed to be used with this system as in Figure 10 so that the pins on the grips and the holes in the specimen can be used for initial alignment.

The specimen ends are fixed by the screws.

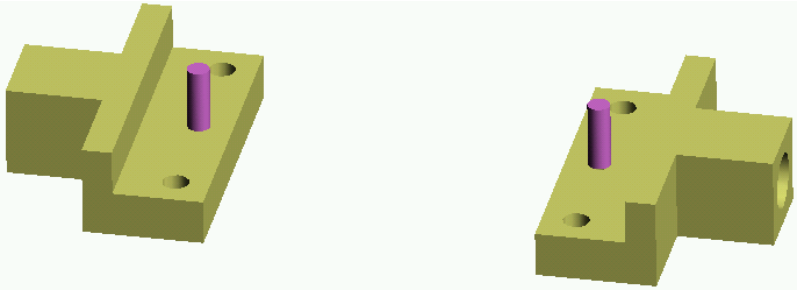

(a)

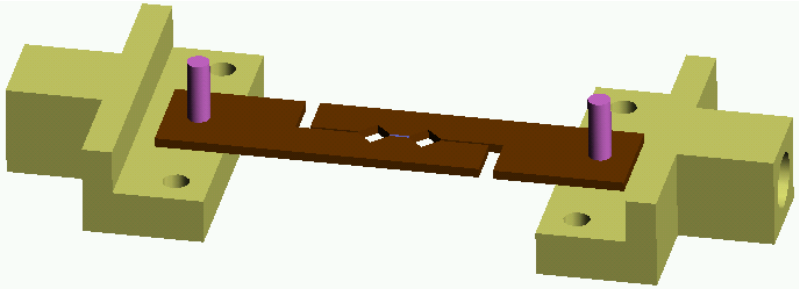

(b)

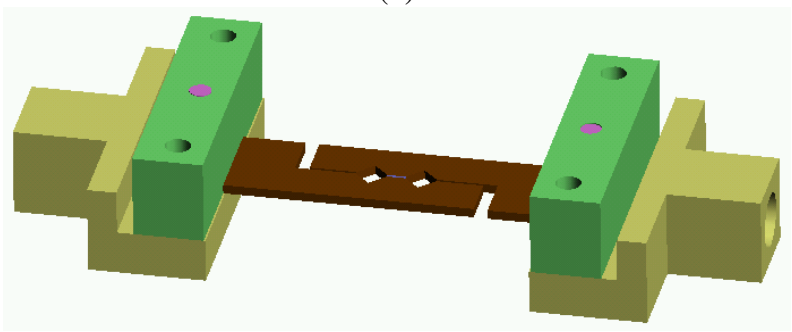

(c)

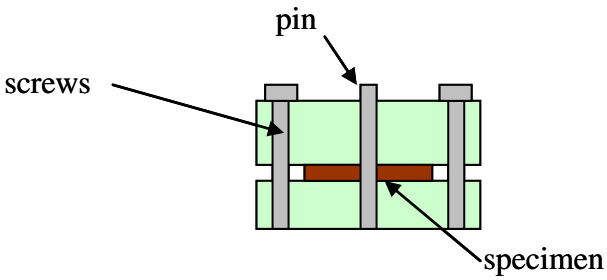

(d)

Figure 10 grip and specimen configuration

2.6 Testing Configuration

Figure 11 is a schematic diagram of testing configuration with Tytron.

Starting from the left, the reaction fixture is fixed; a force transducer measures force applied to the specimen, displacement gage under the actuator measures the movement of the actuator.

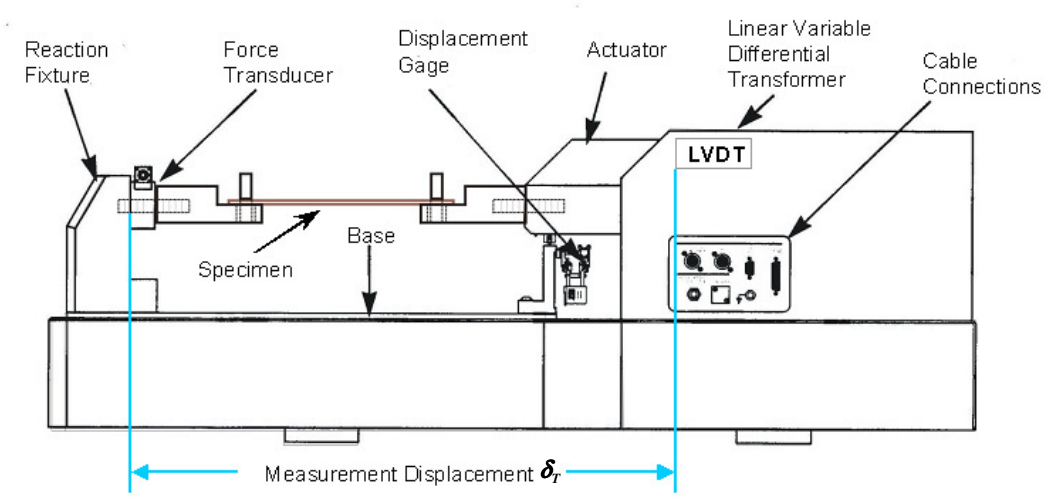

Figure 11 Schematic diagram of testing configuration

The shear lap test is performed using a uniaxial testing machine. The total uniaxial displacement recorded by a displacement sensor can be expressed as

$$\delta_T(P) = P \cdot \left(S_m + S_g + S_a\right) + \delta_n(P) \tag{1}$$

where δ_T is the total or apparent displacement as a function of applied force P, recorded by the displacement sensor; S_m, S_g and S_a are the compliance of testing machine, grip and copper adherend, respectively; δ_n is the net shear displacement of solder.

The net shear displacement can be determined by subtracting the displacements produced by the system compliance from the apparent displacement. In general, the machine and grip compliance are determined experimentally, while the adherend compliance is determined by a Finite Element Analysis. Although possible theoretically, the compensation can produce large systematic errors, especially when

the magnitude of the net shear displacement is small. For example, the net shear displacement is less than 1 μm for the test for an elastic modulus of solder alloys if the height of solder is in the order of a few hundred μm. With the typical uniaxial testing machines, the displacement produced by the system compliance is much greater than the net shear displacement and a small error in compensation can cause a large error in modulus determination. This is motivation of the direct local measurement approach proposed in this work.

Figure 12 shows specimens before and after deformation and these pictures illustrate one of the deformations to be compensated. There is displacement caused by copper compliance and the displacements which need to be compensated are much larger than the shear displacements of solder with 300μm joint height.

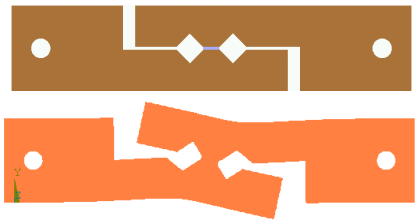

Figure 12 Displacement caused by copper compliance

Figure 13 shows an example when 26N load is applied to the proposed specimen configuration and test configurations. The load is still in the elastic region for the solder alloy used. The blue line is solder only displacement, green line indicates displacement of solder and copper adherend, red line indicates measured displacement in with high temperature configuration which includes not only solder

and copper adherend displacement but also machine and grip compliance. Finally, the pink line indicates same thing for room temperature configuration. The displacement is smaller this case because it has shorter axis than high temperature configuration.

In Figure 13, actual solder joint displacement is around 0.2μm but the total displacement measured δ_T is between 7.3~10.9μm which is about 36 to 55 times of the actual solder deformation.

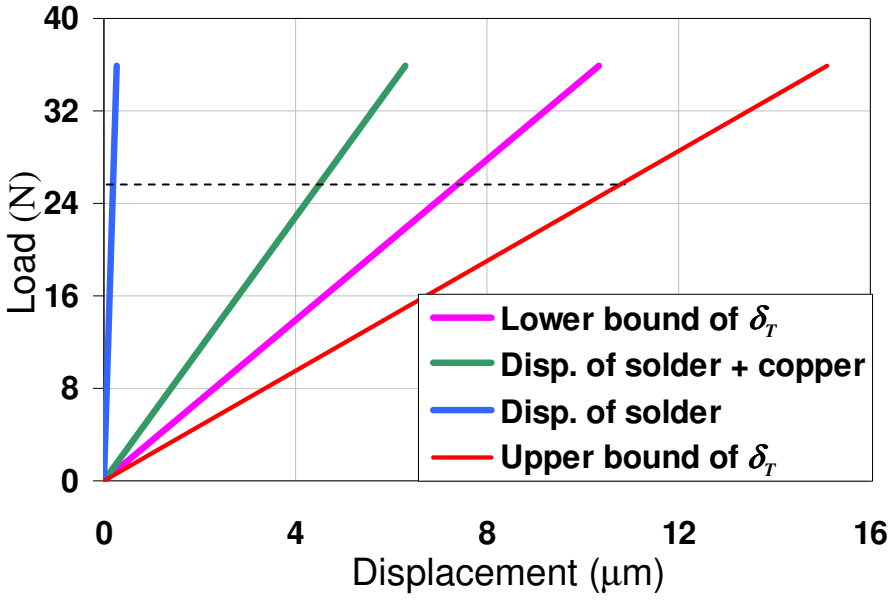

Figure 13 Effect of compliance

Figure 14 (a) and (b) are pictures of room temperature configuration and high temperature configuration respectively.

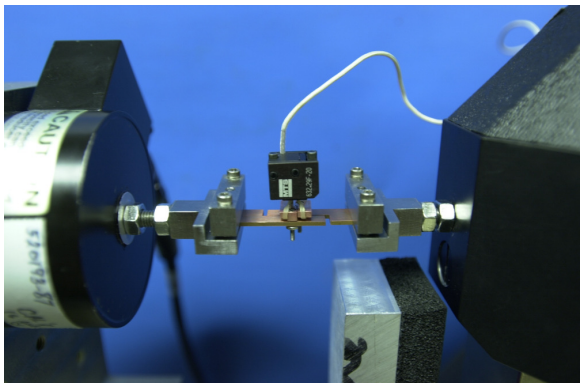

(a) Room Temperature Configuration

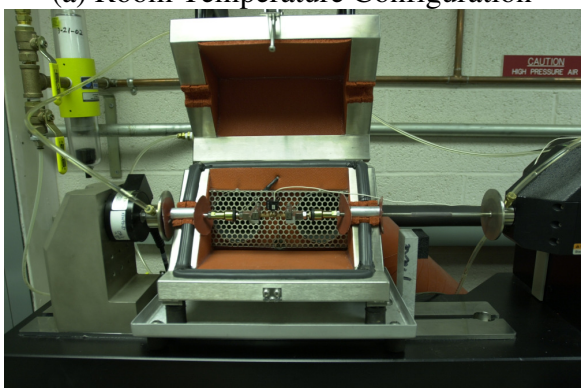

(b) High Temperature Configuration

Figure 14 Testing configurations

2.6.1 High Temperature Testing Configuration

An environmental chamber is implemented in order to accommodate the testing at the elevated temperatures as seen in Figure 15.

A convection oven is chosen in order to achieve uniform temperature of the specimen and to avoid disturbance in deformation through direct contact which is likely to happen with conduction oven. Because it is a convection chamber, there is a vibration.

To keep this vibration from propagating through specimen and possibly affecting deformation measurement, a modification of chamber was inevitable.

The chamber is trimmed at both sides to prevent contact between the pull rods and the chamber and silicone rubber pad was also trimmed and inserted around the rod inside and outside of chamber to keep the inside air from flowing outside. Also the chamber insulation is trimmed to ensure non-contact between the chamber and the pull rods.

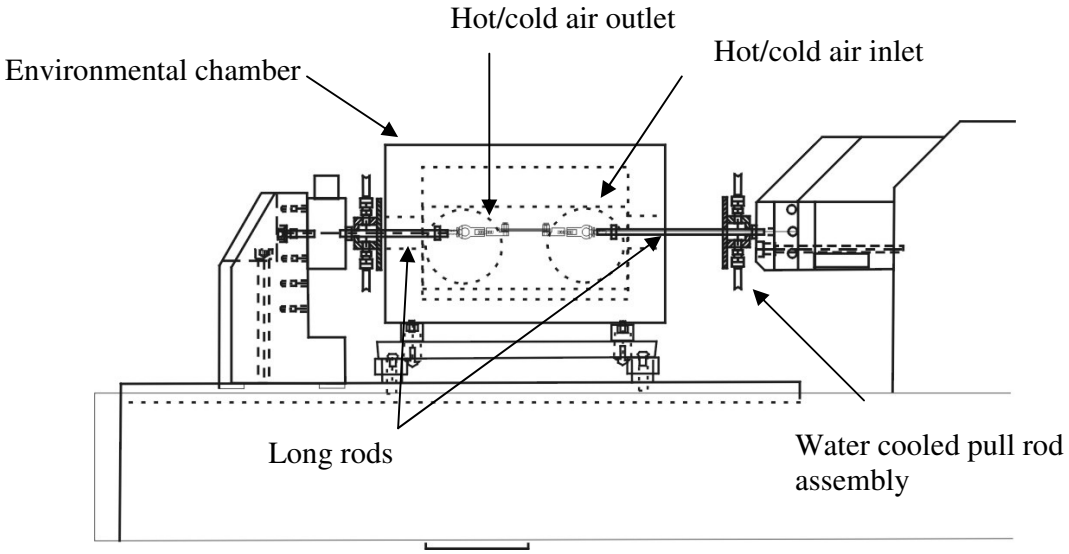

(a)

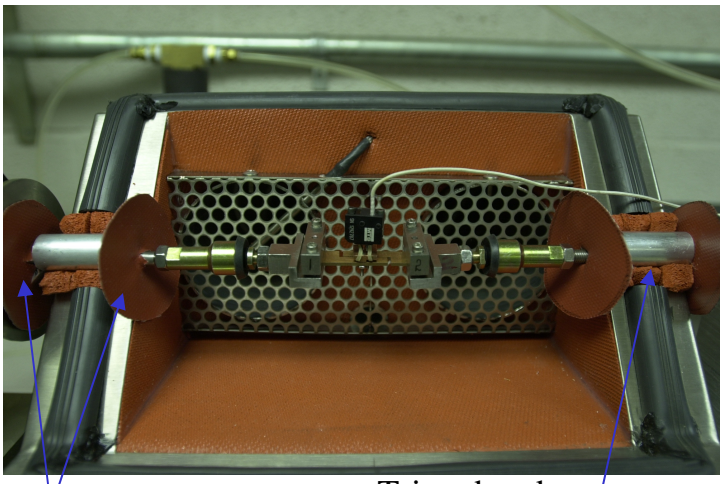

(b)

Figure 15 Elevated temperature test configuration

The rubber band used to attach extensometer to extended unit has to be modified since the regular rubber band provided with extensometer cannot survive long enough at the elevated temperatures. A simple experiment was performed and it turned out the regular rubber band provided with the extensometer is no longer elastic after 10 hours under 130°C. The regular rubber band is replaced with Silicone rubber band which has 450% elongation, 800psi tensile strength and -62°C to 218°C operating temperature range.

2.7 Direct Local Measurement

In the proposed approach, an auxiliary device (referred to as *extension unit*) is attached directly to the specimen. The extension unit is shown in Figure 16 with

relevant dimensions. A hardened stainless steel dowel pin is inserted in the copper plate by press-fit and the unit is attached to the other end of the pin using an epoxy adhesive, as illustrated in Figure 17 a. Figure 17 b illustrates the final assembly where a pair of units is attached to each side of the specimen. A high-resolution miniature extensometer is mounted on the units in such a way that each knife-edge of the extensometer is sitting on each unit while positioning the knife edges symmetrically with respect to the solder. The position of the extensometer is illustrated schematically in Figure 17 c. It is to be noted that the pins are positioned not directly at the top and bottom of the solder. This arrangement is necessary not to disturb the deformations around solder and to accommodate the extensometer.

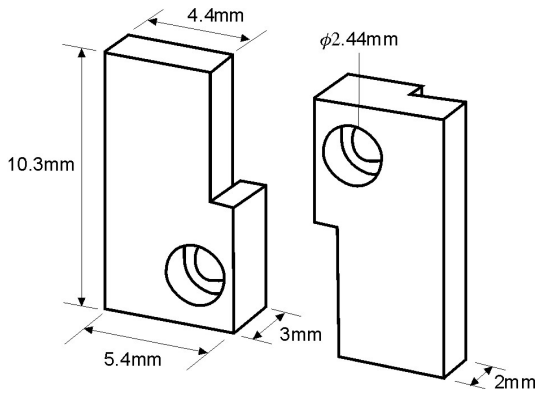

Figure 16 Extension Units.

When the solder experiences a shear deformation, the right-hand side extension unit will have a relative horizontal motion with respect to the left-hand side unit. Figure 18 shows that the unit converts the local shear displacement to the axial displacement, which is recorded by the extensometer. The experimental setup with the testing machine (MTS Tytron) is shown in Figure 19. The high-resolution miniature extensometer (MTS 632.29F-20) is attached to the units by two rubber

bands. With this configuration, a precise control of displacement or strain rate becomes possible.

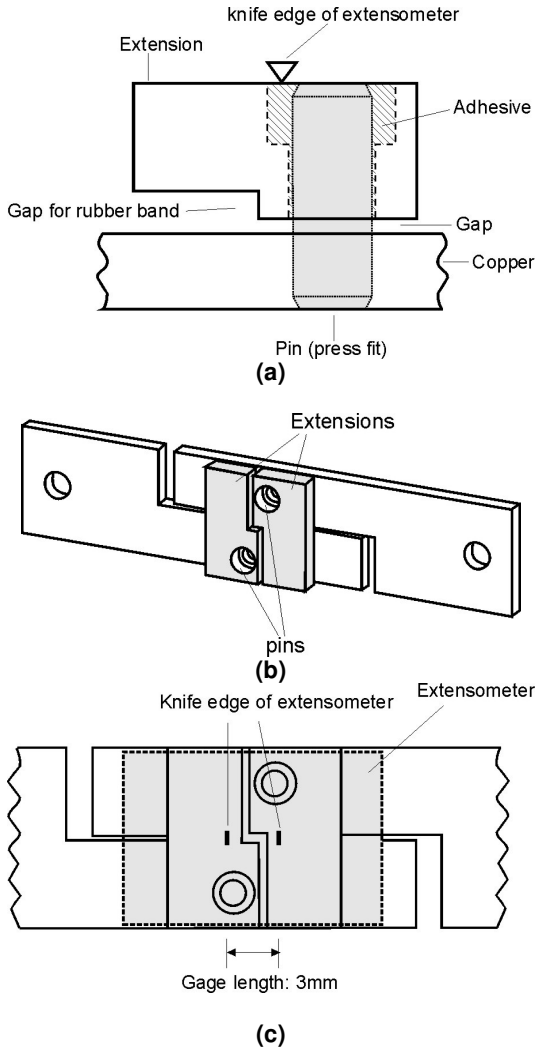

Figure 17 (a) Cross sectional view of the assembly, (b) specimen assembly with extension unit, and (c) position of the knife edges of extensometer.

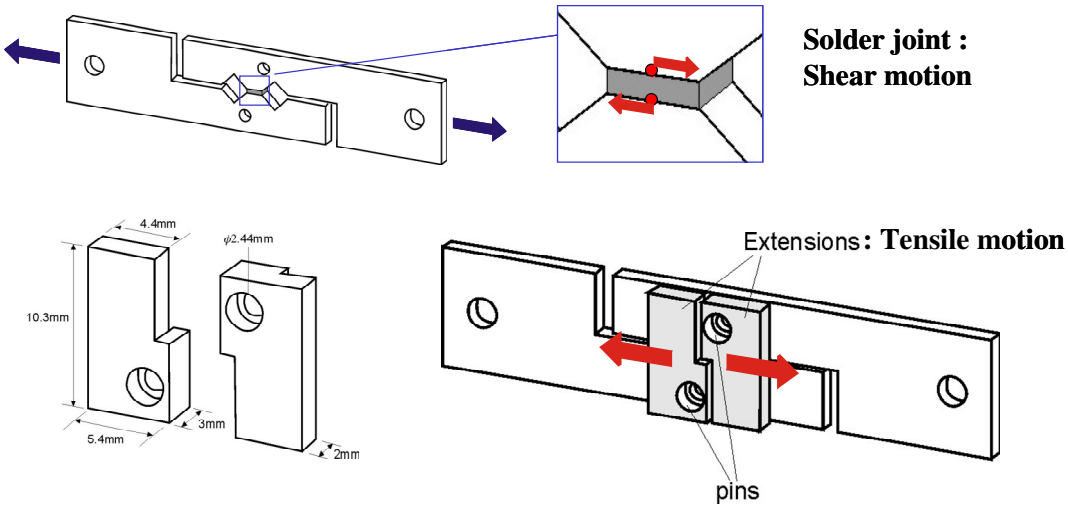

Figure 18 Converting shear displacement to axial displacement

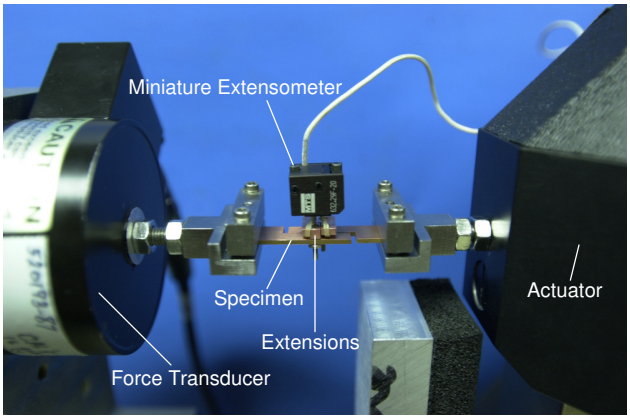

Figure 19 Experimental setup.

2.8 Compensation for Copper Compliance

With the proposed configuration, the only compensation needed is the deformation of the small portion of the copper between the pins while the conventional method needs to compensate the machine, grip and the entire copper plate compliance.

Figure 20 a illustrates the details. The displacement between AA′ ($\delta_{AA'}$) is sought while the extensometer measures the displacement between BB′($\delta_{BB'}$). The deformation of the copper regions AB and A′B′ must be subtracted from the displacement measured by the extensometer. A 2-D finite element analysis was used to determine the amount of displacement to be compensated (referred to *compensation displacement*). The mesh used for the analysis is shown in Figure 20 b.

The deformed configuration of the specimen is illustrated in Figure 20 c, where the deformation is greatly exaggerated. A large rigid-body rotation of the gage section is evident. This rigid-body rotation produces a substantial amount of apparent axial displacement when the conventional uniaxial test is used, which must be compensated from the measured displacements. It is important to note that the extension units rotate together with the gage section and thus this effect is greatly reduced with the proposed configuration.

Figure 20 d exaggerates the deformation in Figure 20 b. It is magnified view of the area around solder joint after deformation. The compensation can be expressed as a function of θ_1, θ_2, and h as follows.

$$\delta_{AA'} = \delta_{BB'} - 2h(\theta_1 - \theta_2) - 2\delta_{AB} \tag{2}$$

θ_1: rigid body rotation of the solder

θ_2: rotation of the pin

h: vertical distance between the pin and the solder joint

δ_{AB}: displacement between A and B caused by copper deformation

θ_1, θ_2 and δ_{AB} can be obtained from FR modeling.

The compensation displacement is a function of the applied force and the thickness of the copper plate. It is worth noting that it is not affected by the modulus of solder material but it is strongly influenced by the modulus of the copper. The modulus of copper plate used in the test was obtained experimentally using a copper strip specimen with strain gages and the value at room temperature was 104.66 GPa, which was slightly smaller than the value in the handbook.

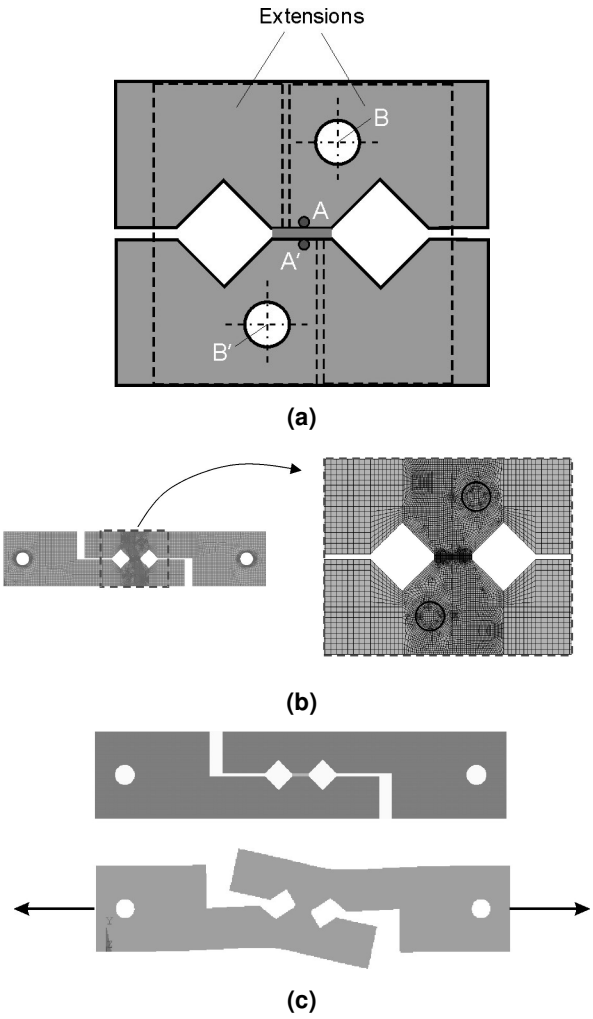

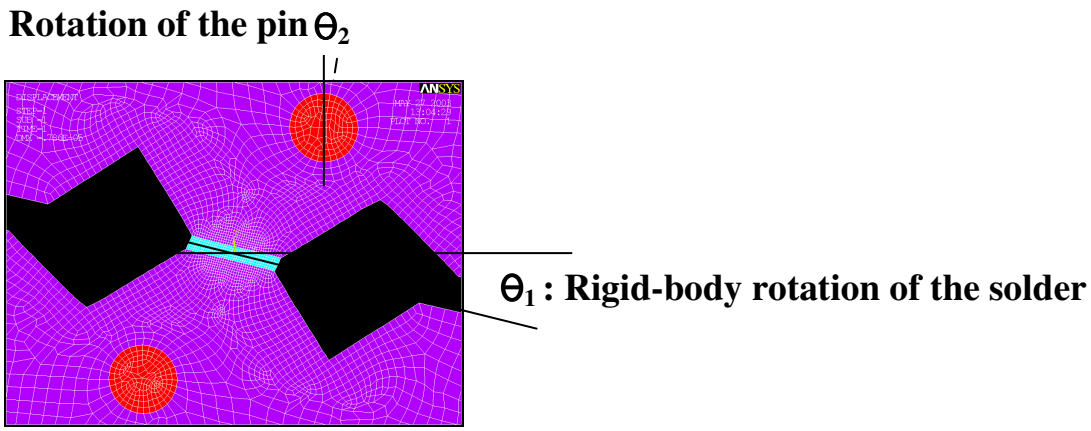

(d) rotation of the solder and pin

Figure 20 (a) Relative position of the pins with respect to solder, (b) FEM mesh used to determine the amount of compensation, and (c) deformed configuration of the specimen subjected to an axial loading. (d) rotation of the solder and pin respectively

The compensation rate, defined as the compensation displacement per unit load, is plotted as a function of thickness of the copper plate in Figure 21. As expected from the elastic deformation of copper, the compensation rate has a linear relationship with the copper thickness.

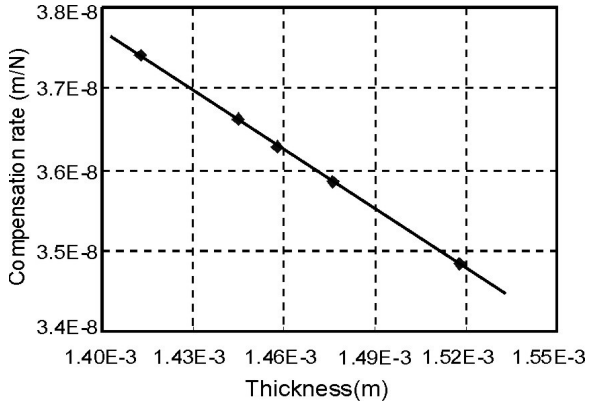

Figure 21 Compensation rate as a function of copper thickness.

Chapter 3: Experimental Results - Constitutive Property Measurements of Sn3.5Ag Solder Alloy

Experiments performed at three different temperatures which were 25ºC, 75 ºC, 125 ºC and seven different strain rates, $1\times10^{-1}s^{-1}$, $1\times10^{-2}s^{-1}$, $1\times10^{-3}s^{-1}$, $1\times10^{-4}s^{-1}$, $1\times10^{-5}s^{-1}$, $1\times10^{-6}s^{-1}$ $1\times10^{-7}s^{-1}$. Modulus tests were performed and followed by constant strain rate tests. The effect of compensation was investigated both for modulus test and constant strain rate test.

3.1 Experimental Results

3.2.1 Modulus test

The proposed scheme was implemented to measure the elastic modulus of a binary lead-free solder (Sn3.5Ag). The specimen was fabricated with the solder with a nominal height of 300 μm. Each specimen was polished after reflow and the actual height of the solder was measured using an optical microscope. The copper plate has a slight variation in thickness after polishing. The thickness was also measured for each specimen to employ a correct compensation rate shown in Figure 22.

The specimen was subjected to a constant strain rate of $\dot{\gamma} = 1\times10^{-3}/\sec$. A representative force vs. strain plot obtained at 25°C is shown in Figure 22.The plot clearly indicates the stability of the proposed configuration. The shear modulus was determined from the plot, and subsequently it was converted into the Young's

modulus using the relationship of the elastic constants. The Poisson ratio of pure Tin ($\nu = 0.33$) was used in the conversion.

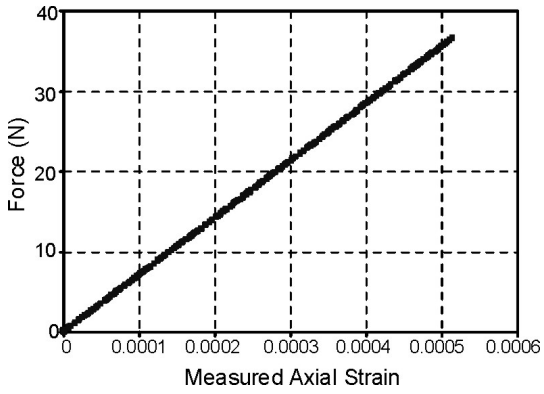

Figure 22 Force-strain plot for modulus test.

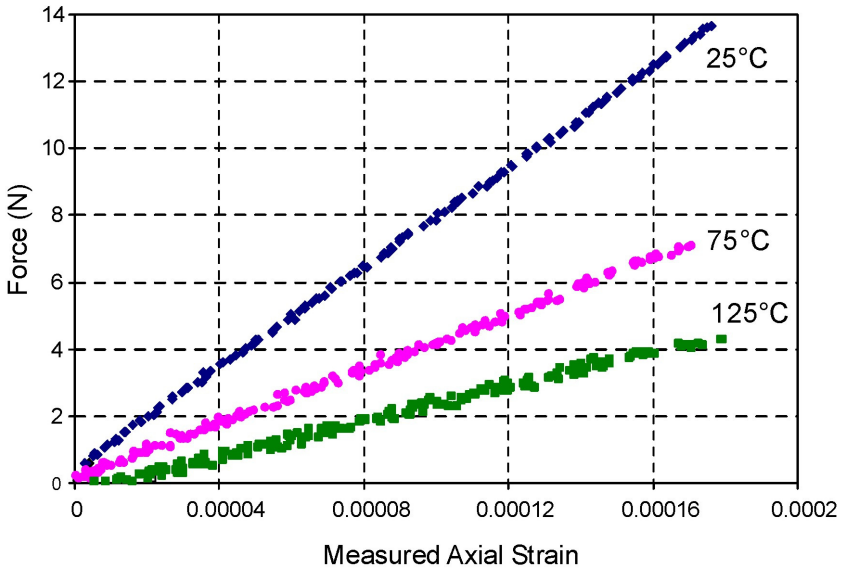

Figure 23 Modulus test results with a shear strain rate of 1E-3/sec

Specimen-to-specimen variations in modulus were inevitable. The number of tested specimens was 32 and the results indicated a normal distribution. The average value was taken to represent the data and it was 42.8 GPa, which is slightly higher than the modulus of pure Tin reported in the literature ($E_{Sn} = 41.4$ GPa).

3.2.2 Constant Strain Rate Test

In general, a rate-dependent plastic behavior can be characterized by a data set consisting of a steady-state strain rate and a saturation stress. The data are usually obtained from constant load (or creep) tests. In this research, however, the constant strain rate tests were conducted to obtain the data set.

As a load increases at a constant strain rate, the plastic flow reaches the steady state condition, where the stress becomes saturated, and thus both strain rate and stress are constant. This is similar to the secondary creep during constant load tests.

The constant strain rate test has advantages over the creep test. With the constant strain test, rate-dependent properties as well rate-independent properties can be determined, which can reduce the total number of tests significantly. Another practical advantage is that undesired data can be screened out at the early stage of the tests. If the specimen has defects and thus a crack grows during the test, a significant load drop is resulted. Since a low strain rate test usually runs for 40~60 hours, it is extremely time-effective if the specimen with defects is detected at the early stage of test. Figure 24 shows an example of the load-strain curve when an undesired crack propagates along the solder/copper interface. A significant load drop is evident. The microscopic view of solder area of the specimen is also shown in Figure 24.

The tests with constant strain rates ranging from 10^{-1}~10^{-8}/sec were conducted at 25°C, 75°C and 125°C. For the constant strain rate tests, the bending effect associated with misalignment of the specimen is not significant because sufficient plastic flow occurs during the test to eliminate the effect [12](ASTM standard).

Consequently, only one side of the specimen was measured for the constant strain rate test. Figure 25 shows a typical load-strain curve obtained from the constant strain rate test.

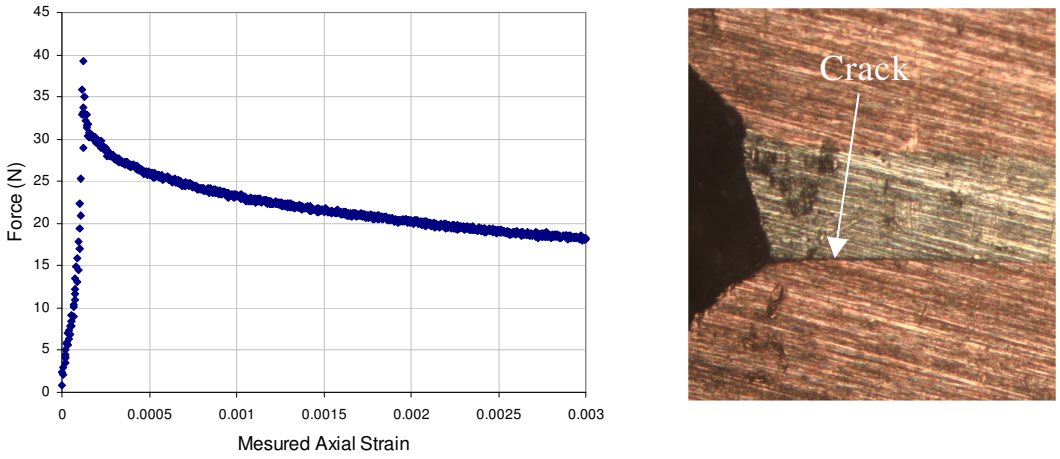

Figure 24 Load-strain curve when crack propagates along the copper /solder interface

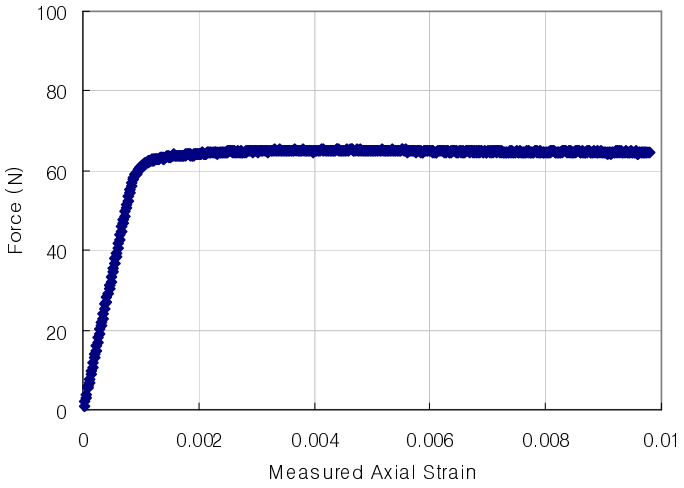

Figure 25 Force-strain curve from constant strain rate test ($\dot{\gamma} = 2.89 \times 10^{-6}$/sec , T=25°C)

3.3 Effect of Compensation

In the section, the effect of compensation is discussed by comparing the conventional method with direct local measurement scheme proposed in chapter 2.

3.3.1 Effect of Compensation on a Modulus Test

The effect of compensation in modulus test is shown in Figure 26.

As you see in this figure, load versus compensation, the amount of compensation needed for direct measurement, which is pink line here, is much smaller than the compensation needed for conventional approach.

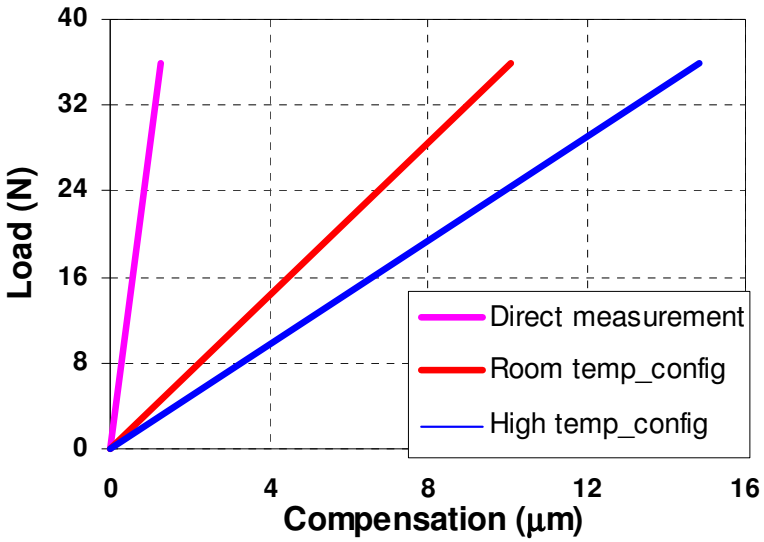

Figure 26 Effect of Compensation

As a consequence, for 1% error of compensation, the modulus of solder measured by direct measurement will have error boundary from 95.6% of E_{true}, which is the true solder modulus to 104.8% of E_{true}. Whereas the solder modulus measured

by convention method have much larger error boundary, for room temperature configuration from 73.3% of E_{true} to 157.1% of E_{true} and for high temperature configuration from 65.2% of E_{true} to 215.0% of E_{true}.

As results, it is concluded that the modulus can be measured much more accurately by the direct local measurement scheme proposed in chapter 2.

3.3.2 Effect of Compensation on a Constant Strain Rate Test

As we mentioned in chapter 2.5 Testing Configuration, the total displacement measured by conventional method includes not only net shear displacement of solder but other compliances.

$$\delta_T(P) = P \cdot (S_m + S_g + S_a) + \delta_n(P) \tag{3}$$

where δ_T is the total or apparent displacement as a function of applied force P, recorded by the displacement sensor; S_m, S_g and S_a are the compliance of testing machine, grip and copper adherend, respectively; δ_n is the net shear displacement of solder again.

By taking a derivative with respect to time and dividing by height of solder joint Δh, we obtain Equation (5) which shows the relationship between apparent shear strain rate $\dot{\gamma}_T$ and net shear strain rate of solder $\dot{\gamma}_n$.

$$\frac{\dot{\delta}_n}{\Delta h} = \frac{1}{\Delta h}\left\{\dot{\delta}_T - \dot{P} \cdot (S_m + S_g + S_a)\right\} \tag{4}$$

$$\dot{\gamma}_n = \dot{\gamma}_T - \frac{\dot{P}}{\Delta h} \cdot (S_m + S_g + S_a) \tag{5}$$

In typical constant strain rate test, the rate of applied load changes with time, therefore the true shear strain rate of solder also changes with time.

Figure 27 below is one of constant strain rate test results showing load versus time. In this load versus time chart, load is increasing linearly for certain time and in this evolution region which marked with a red circle, plastic flow develops and the load rate is changing abruptly and becoming constant as the flow gets saturated.

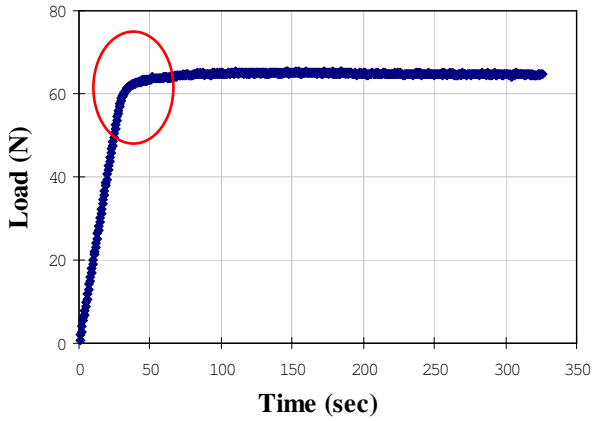

Figure 27 Force-time plot for constant strain rate test

Figure 28 is a shear strain versus time chart. In this chart, the blue line is the apparent shear strain and the red line is the actual shear strain. As you see in this chart, even though the apparent shear strain increases linearly the actual strain at solder joint is not increase linearly.

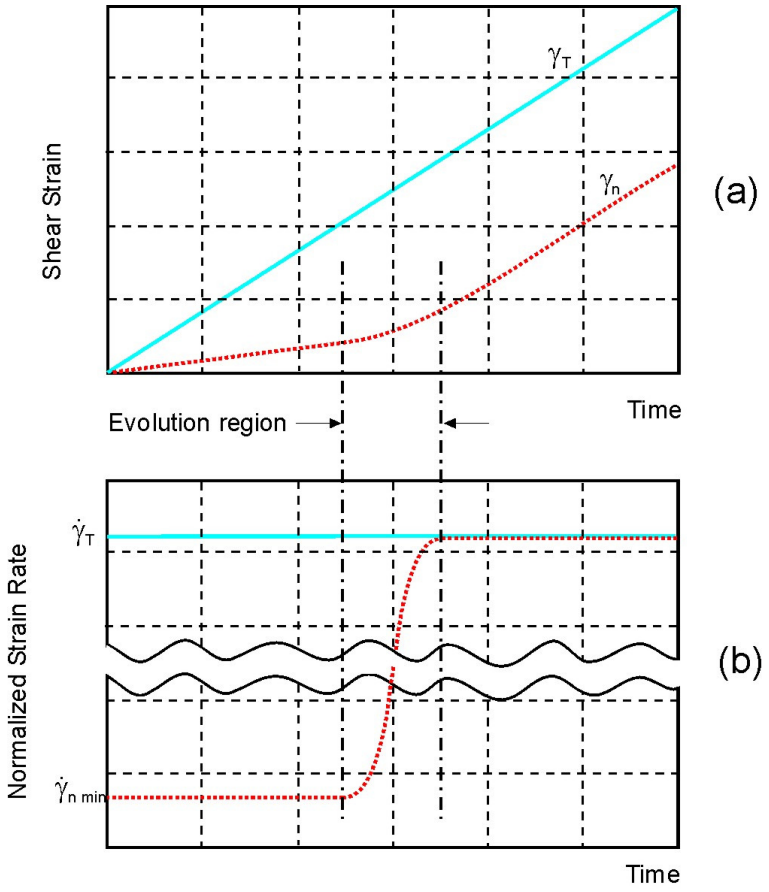

Figure 28 Illustration of the effect of compensation on the constant strain rate test. Apparent and net (a) shear strain and (b) shear strain rate as a function of time.

In conventional approach, this strain rate jump can affect on saturated stress significantly since $\dot{\gamma}_{n\min} \cong \frac{\dot{\gamma}_T}{40} \sim \frac{\dot{\gamma}_T}{60}$

If this effect of strain rate jump is concerned, creep test can be an alternative..

$$\dot{\gamma}_n = \dot{\gamma}_T - \frac{\dot{P}}{\Delta h} \cdot \left(S_m + S_g + S_a \right) \tag{6}$$

As you see in the above equation, in creep test, $\dot{P} = 0$ therefore $\dot{\gamma}_n = \dot{\gamma}_T$

But the creep test can be extremely time-consuming because the possible defect in the specimen or other factors that disturb the experimental data cannot be identified until the experiment is completed.

Figure 29and the following chart show a great example.

In Figure 29, there is a crack in the specimen between solder and copper.

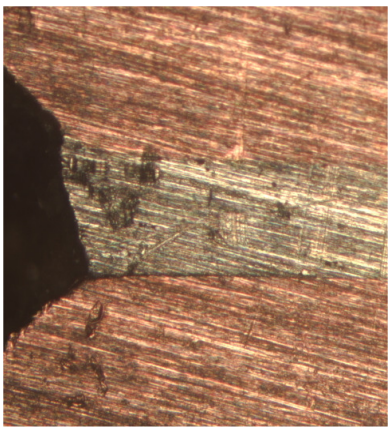

Figure 3.8

Figure 29 Micrograph showing a crack propagated along the copper/solder inter face during loading

Figure 30 (a) illustrates an example. The figure (a) shows results from two creep tests with the identical load. The higher strain rate was caused by an undesired crack. Figure (b) is constant strain rate test result for the case with an undesired crack.

In the strain versus time chart below, the blue line is the result when there is a crack. Even in this blue line, there is secondary creep region with constant creep strain rate just like ideal specimen without a crack. Whereas in constant strain rate test case, the stress will drop immediately as you see in Figure 30 (b).

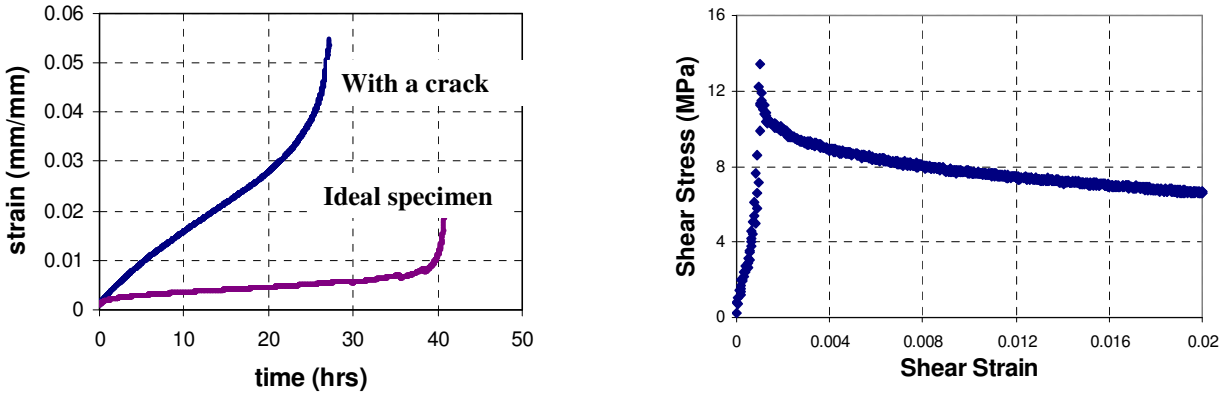

Figure 30 Illustration of load drop (a) time and strain plot, (b) stress-strain plot

Chapter 4: Constitutive Properties of Sn96.5Ag3.5

4.1 Constitutive Models

Constitutive models relate deformation in a material to the applied force. One of the simplest constitutive models is elastic model where the stress and strain is linearly proportional. The elastic model will be enough to describe the materials behavior for the isotropic linear elastic material. But in real life, the engineering materials are a lot more complex to describe the behavior with elastic model. The stress does not only depend on strain but also on strain rate, temperature and other factors. The constitutive model in equation (7) is based on the simple concept that the flow stress is only a function of instantaneous values of strain, strain rate and temperature. But for the material which experiences significant irreversible plastic deformation, the flow stress not only depends on the moment values of strain, strain rate and temperature, but also depends on the history of them too.

$$f(\sigma, \dot{\varepsilon}, \varepsilon, T) = 0 \tag{7}$$

$$d\sigma = \left\{\frac{\partial \sigma}{\partial \varepsilon}\right\}_{\dot{\varepsilon}T} d\varepsilon + \left\{\frac{\partial \sigma}{\partial \dot{\varepsilon}}\right\}_{\varepsilon T} d\dot{\varepsilon} + \left\{\frac{\partial \sigma}{\partial T}\right\}_{\varepsilon\dot{\varepsilon}} dT \tag{8}$$

where ε is the uniaxial or equivalent strain, σ is the equivalent stress, T is temperature, and $\dot{\varepsilon}$ is the strain rate.

Typical solder material has high homologous temperature even at room temperature and experiences significant irreversible plastic deformation at operating condition. The deformation is highly dependent on temperature and rate therefore it is

considered viscoplastic material. The behavior of viscoplastic material can be described with two different approaches which are partitioned model or unified model. The partitioned approach divides deformation into three different types, Elastic, time-dependent creep and plastic are those. Then it describes behavior as a sum of elastic deformation, rate-dependent creep, rate-independent plasticity. Whereas unified viscoplastic model, all inelastic deformations are rate-dependent and occurs at all non-zero stress level. In this approach, elastic deformation is still distinguished from inelastic deformation but plastic strain and creep strain are separable. Instead it uses internal state variable, which represents the resistance of the material to inelastic deformations. It doesn't have explicit yield surface and the loading and unloading criterion. [13]

4.2 Determination of Constants

4.2.1 Partitioned Model

The partitioned model can be described as

$$\varepsilon(t) = \varepsilon_{el} + \varepsilon_{pl} + \varepsilon_{cr}(t) \tag{9}$$

where ε_{el} is elastic strain, ε_{pl} is rate-independent plastic strain and ε_{cr} is creep strain.

Recoverable elastic deformation response of solder materials is modeled using the standard Hookean elasticity model. The elastic (or shear) modulus decreases with temperature increasing. The modulus is usually shown to have linear relationship

with temperature [14]. Rate-independent plastic deformation is usually described by a power law relationship [5]. Rate-dependent creep deformation is described by the Weertman's steady state power law.

4.2.1.1 Elastic Properties

The rate-independent elastic behavior can be explained by Hooke's law, and Young's modulus E can be expressed by a linear function of temperature as

$$\sigma = E\varepsilon \qquad E = E_0 - E_1 T \tag{10}$$

where E_0, E_1 are constants and T is temperature in Celsius.

Due to the extremely small strain to be measured for the modulus test, specimen-to-specimen variations were observed. For each temperature, 36 specimens were tested. The results showed a normal distribution and the average value was taken to represent the data. The statistical distribution of the displacements measured at 26N is shown in Figure 31. The normal distribution is evident. Averaging the raw data minimizes possible random errors. From the averaged data, a linear line representing the load-displacement curve was obtained.

After subtracting the compensation displacement, the true load-displacement curve was obtained. It was converted to the shear stress-shear strain curve using the geometrical parameters of the solder joint, from which the shear modulus was determined. Subsequently Young's modulus was calculated by using the relationship of the elastic constants, where Poisson ratio ν was assumed to be 0.33. The elastic properties obtained from experiments at various temperatures were shown in Table 2.

From the results in Table 2, the constants (E_0 and E_1) of Eq. (11) were determined by fitting the curve with linear line, as illustrated in Figure 32.

$$E = E_0 - E_1 T = 48.8 - 0.184T \tag{11}$$

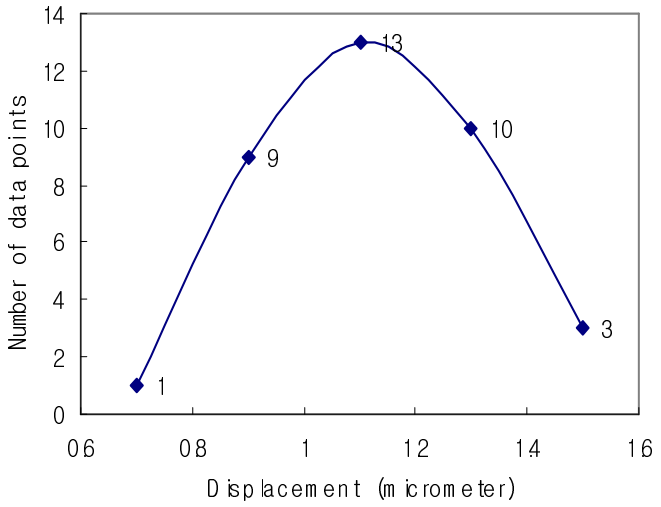

Figure 31 Histogram of measured displacement data

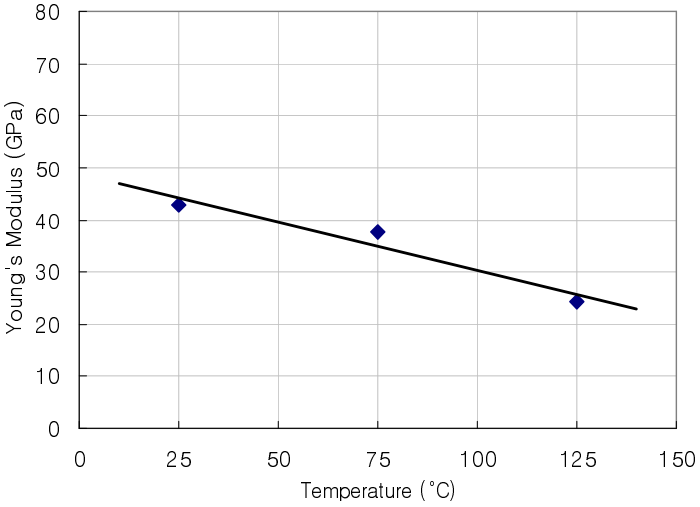

Figure 32 Temperature dependency of Young's modulus

Table 2 Elastic Properties of Sn3.5Ag binary solder

Temperature (℃)	Shear Modulus, G (GPa)	Young's Modulus, E (GPa)
25 ℃	16.1	42.8
75 ℃	14.2	37.8
125 ℃	9.19	24.4

4.2.1.2 Rate-independent Plastic Properties

The exponential hardening model can be expressed as

$$\sigma = K\varepsilon^{n_p} \quad \text{for } \sigma > \sigma_y \tag{12}$$

where the pre-exponential coefficient *K* and plastic strain hardening exponent n_p can be obtained by fitting the stress-strain curve beyond the stresses exceeding the yield stress σ_y .Since the solder material has a high homologous temperature, time-dependent creep behavior is dominant at a low strain rate ($\dot{\gamma} = 1\times10^{-7} \sim 1\times10^{-8}$). However, the time dependent deformation can be observed even with a relative high strain rate ($\dot{\gamma} = 1\times10^{-1} \sim 1\times10^{-2}$). Consequently, it is difficult to obtain time-independent plastic properties from the simple tensile testing machine.

In 1997, Mavoori et al. [15] proposed an extrapolation technique to obtain rate-independent plastic properties. The plastic shear strain-shear stress curves with various strain rates are shown in Figure 33, where the elastic strains were subtracted from the total strains using the 0.2% strain offset. Using the data shown in Figure 33, the shear stresses were plotted as a function of the shear strain rate and the results are

shone in Figure 34. By extrapolating the curves in Figure 34, the rate-independent stress-strain curve for Sn3.5Ag binary solder was plotted at various temperatures in Figure 35. Assuming von Mises yield criterion, the shear stress and shear strain can be converted to the tensile stress and tensile strain using the following relations:

$$\sigma = \tau\sqrt{3} \qquad \varepsilon = \frac{1}{\sqrt{3}}\gamma \tag{13}$$

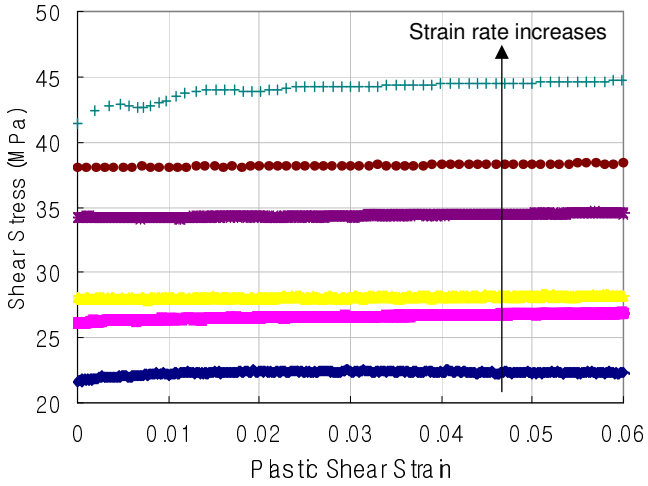

Figure 33 Plastic shear strain vs. shear stress for various strain rates ($T = 25°C$)

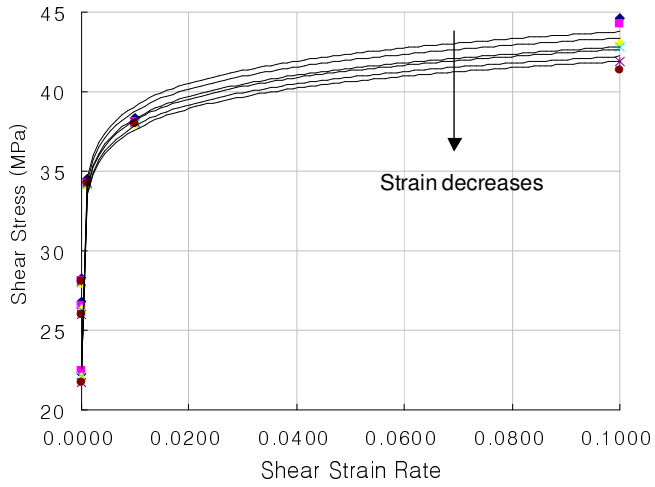

Figure 34 Shear strain rate vs. shear stress for various strains ($T = 25°C$)

From the data plotted in Figure 35, Time-independent constants (K and n_p) of Equation (14) can be obtained using linear curve fitting (Figure 36 a and b).

$$K = 286.04 - 0.579T(°K)$$
$$n_p = 0.000203T(°K) - 0.03998 \quad (14)$$

and Equation (12) can be written as

$$\sigma = K\varepsilon^{n_p} = \left(286.04 - 0.579T\right)\varepsilon^{(0.000203T - 0.03998)} \quad (15)$$

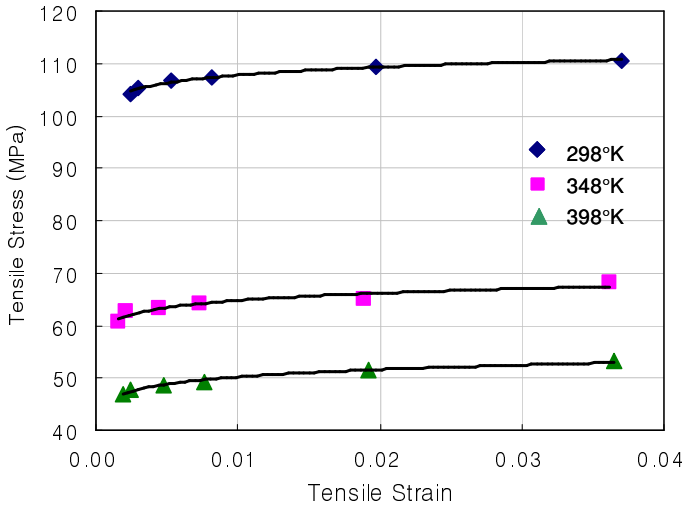

Figure 35 Time-independent stress-strain curves for Sn3.5Ag solder at various temperatures

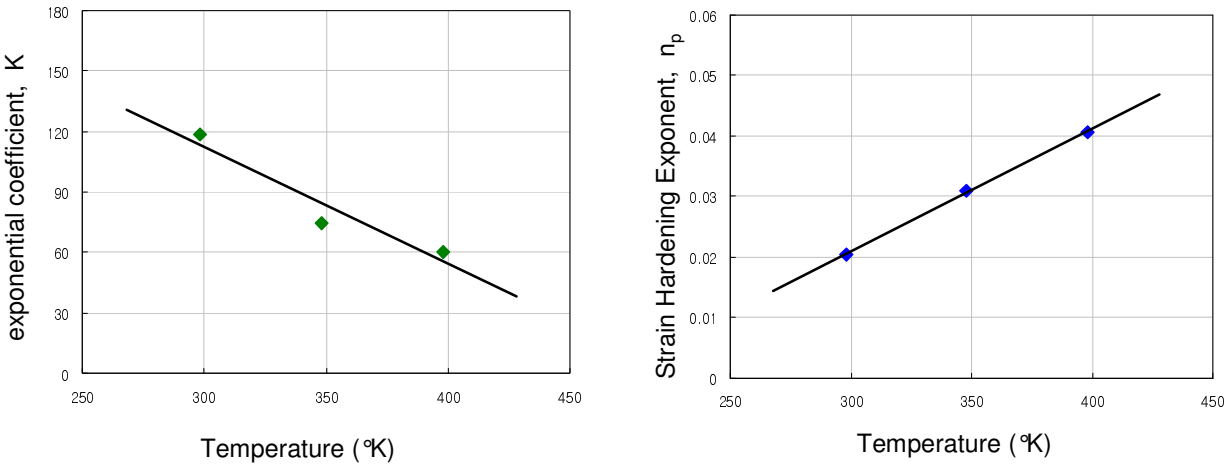

(a) (b)

Figure 36 Temperature dependency of time-independent constants (a) *K* (b) n_p

Rate-dependent Creep Properties

For the time-dependent creep behavior, the Weertman's steady state power law has been widely used because of its simplicity. The creep strain rate can be written as

$$\dot{\varepsilon}_{cr} = A\sigma^{\frac{1}{n_c}} e^{\frac{-Q}{RT}} \qquad (16)$$

where A is creep constant, n_c is creep strain hardening exponent, Q is creep activation energy and R is universal gas constant. In this study, a single power law was used because the power law breakdown was not observed in the test data. Table 3 summarizes the test data obtained by the constant strain rate tests at different temperatures. By taking logarithms on both sides, equation (16) can be written as

$$\ln \dot{\varepsilon}_{cr} = \ln A - \frac{Q}{RT} + \frac{1}{n_c} \ln \sigma_v \qquad (17)$$

Table 3 Constant strain rate test data

T=298°K	**τ (MPa)**	**dγ/dt**
1	46.30	1.00×10^{-1}
2	38.33	1.00×10^{-2}
3	35.55	1.00×10^{-3}
4	28.89	1.00×10^{-4}
5	27.53	1.00×10^{-5}
6	22.44	2.89×10^{-6}
7	17.40	1.96×10^{-7}
8	12.90	2.47×10^{-8}
T=348°K	**τ (MPa)**	**dγ/dt**
1	21.70	1.00×10^{-3}
2	20.21	1.00×10^{-4}
3	15.30	1.00×10^{-5}
4	14.01	1.00×10^{-6}
5	9.50	1.00×10^{-7}
T=398°K	**τ (MPa)**	**dγ/dt**
1	18.84	1.00×10^{-2}
2	13.37	1.00×10^{-3}
3	12.30	1.65×10^{-4}
4	10.61	2.54×10^{-5}
5	6.91	3.56×10^{-6}
6	6.41	1.00×10^{-6}
7	5.38	1.00×10^{-7}

After converting the data in Table 3 into the normal components, they were plotted using equation (17). The log plot is shown in Figure 37. From the y-intercepts and the slopes, $lnA\text{-}Q/RT$ and $1/n_c$ can be obtained, respectively. Figure 38 shows the temperature dependent creep strain hardening exponent $1/n_c$, which can be expressed by a linear function as

$$\frac{1}{n_c} = 22.354 - 0.0340T \qquad (18)$$

The constants *A* and *Q/R* can be decomposed by plotting *lnA-Q/RT* with respect to *1/T* as shown in Figure 39. The creep constant A and Q/R obtained from the y-intercept and slope were

$$A = 3.628\times10^{11}, \qquad \frac{Q}{R} = 25158 \qquad (19)$$

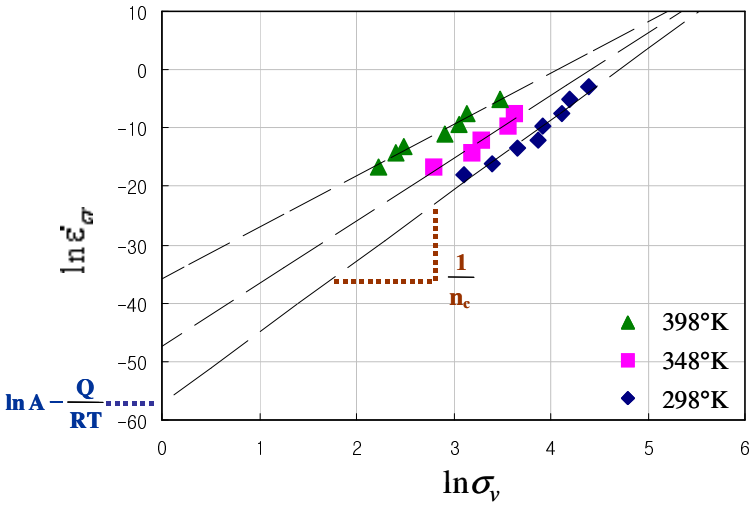

Figure 37 Logarithmic plot of test data

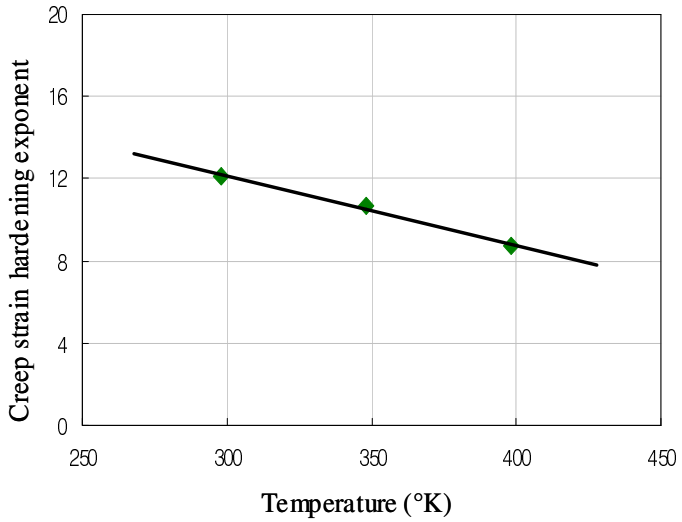

Figure 38 Creep strain hardening exponent vs. temperature

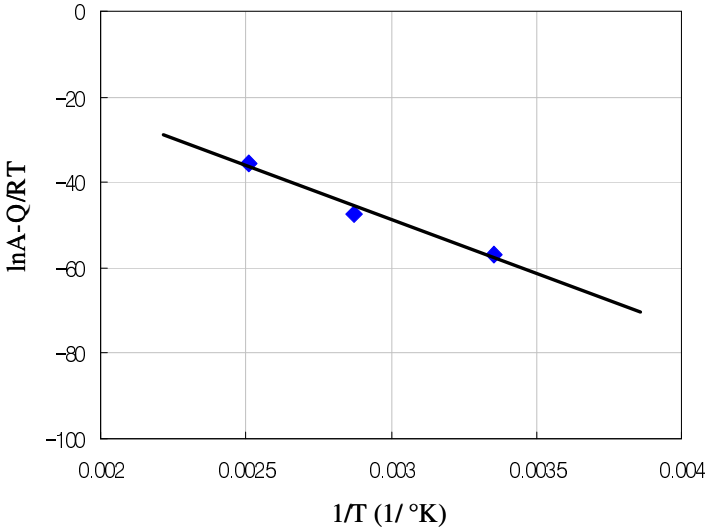

Figure 39 Determination of *A* and *Q/R*

4.2.2 Unified Model

Pugh and Robinson in 1978 found an experimental evidence of inherent rate-dependency and creep-plasticity interactions on structural alloys at elevated

temperatures, which implied that the inelastic deformation was controlled by a single overall mechanism and this it could be treated in a unified manner[16].

Anand model is one of the unified models and it was initially formulated for the metal hot working process to simulate large visco-plastic deformations at extremely high temperatures [13]. Recently, several researchers [4, 17-20] have applied Anand model to the behavior of the solder alloys. Governing equations of Anand model can be written as:

Flow Equation

$$\dot{\varepsilon}_p = \dot{\varepsilon} = A \exp\left(-\frac{Q}{RT}\right)\left[\sinh\left(\xi \frac{\sigma^*}{s^*}\right)\right]^{1/m} \tag{20}$$

Evolution Equation

$$\dot{s} = \left\{ h_0 \left| 1 - \frac{s}{s^*} \right|^a sign\left(1 - \frac{s}{s^*}\right) \right\} \dot{\varepsilon}_p \tag{21}$$

with

$$s^* = \hat{s}\left[\frac{\dot{\varepsilon}_p}{A}\exp\left(\frac{Q}{RT}\right)\right]^n \tag{22}$$

Anand model contains nine constants and they are summarized in Table 4. Commercially available finite element code such as ANSYS has built-in capabilities of Anand model and it requires these nine constants as input parameters.

Table 4 Parameters in Anand model

Parameter	Unit	Definition	Determined from
A	sec^{-1}	Pre-exponential factor	Flow Equation
Q/R	°K	Activation energy/universal gas constant	
ξ		Multiplier of stress	
$\hat{s}$	MPa	Coefficient for deformation resistance saturation value	
m		Strain rate sensitivity of stress	
n		Strain rate sensitivity of saturation value	
h_0	MPa	Hardening / softening constant	Evolution Equation
a		Strain rate sensitivity of hardening or softening	
s_0	MPa	Initial value of deformation resistance	

Using Equation (22), the flow equation (Equation (20)) can be rearranged for the saturation stress σ^* as

$$\sigma^* = \frac{\hat{s}}{\xi}\left(\frac{\dot{\varepsilon}_p}{A}e^{Q/RT}\right)^n \sinh^{-1}\left[\left(\frac{\dot{\varepsilon}_p}{A}e^{Q/RT}\right)^m\right] \tag{23}$$

From Eq. 17, five material constants, Q/R, A, $\hat{s}/\xi$, m and n can be determined by a nonlinear least square fitting of $\dot{\varepsilon}_p \sim \sigma^*$ data from the experimental results of Table 3. The parameter ξ is chosen such that the constant c is less than unity. Then $\hat{s}$ can be determined from the combination term $\hat{s}/\xi$. The constant c is defined as follows:

$$c = \frac{1}{\xi}\sinh^{-1}\left[\left(\frac{\dot{\varepsilon}_p}{A}e^{Q/RT}\right)^m\right] \tag{24}$$

Figure 40 shows the experimental data with the functions determined by the above analysis.

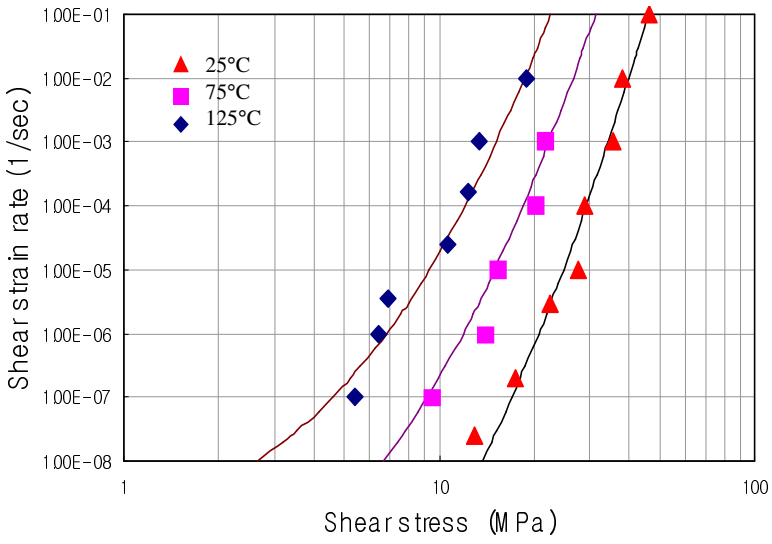

Figure 40 Fitted curves using Anand model for Sn3.5Ag binary solder

The other three constants can be determined from the evolution equation. From Equation (20) and the given relation, $\sigma = cs$, the internal variable of the evolution equation can be expressed in terms of stress as

$$\dot{\sigma} = ch_0 \left(1 - \frac{\sigma}{\sigma^*}\right)^a \dot{\varepsilon}_p \tag{25}$$

or equivalently,

$$\frac{d\sigma}{d\varepsilon_p} = ch_0 \left(1 - \frac{\sigma}{\sigma^*}\right)^a \tag{26}$$

The strain hardening data, which is the slope of stress-plastic strain curve obtained from an isothermal, constant strain rate test, reflect the evolution of the internal variable. Finally, the integrated form of equation (25) can be written as

$$\sigma = \sigma^* - \left[\left(\sigma^* - cs_0\right)^{(1-a)} + (a-1)\left\{(ch_0)\left(\sigma^*\right)^{-a}\right\}\varepsilon_p\right]^{\frac{1}{1-a}} \tag{27}$$

Three material constants h_0, a, and s_0 of Eq. 19 can be determined by applying a nonlinear least square fitting of $\varepsilon_p \sim \sigma$ curves near the transient region. The set of constants were obtained for each constant strain rate test and they were averaged. An example of non-linear curve fitting applied to the transient region is illustrated in Figure 41. All nine Anand constants determined for Sn3.5Ag binary solder are summarized in Table 5.

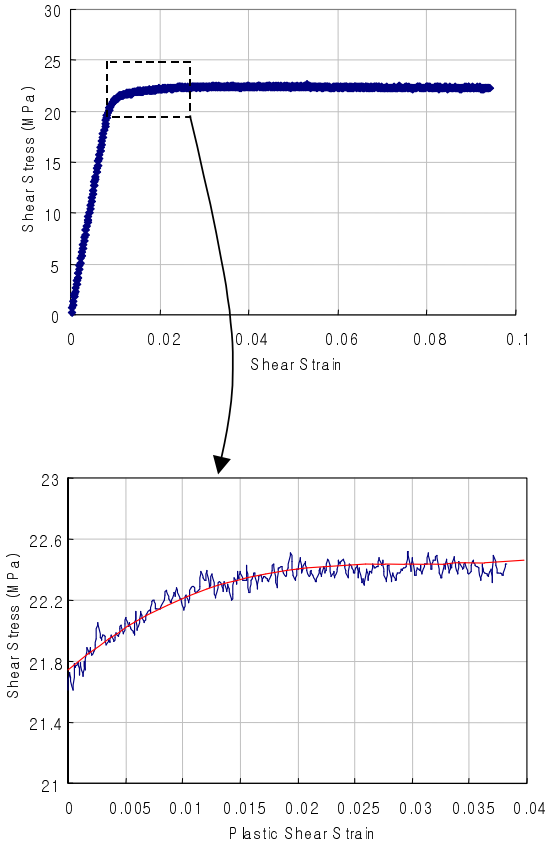

Figure 41 Non-linear curve fitting for the transient region

Table 5 Anand constants

Parameter	Value
A	22452
Q/R	12270
ξ	19
$\hat{s}$	43.03
m	0.5607
n	0.0266
h_0	3327
a	1.2830
s_0	66.85

Chapter 5: Reliability Assessment of Lead-Free Solder Joint - Calibration of Virtual Qualification Model for Leaded Packages with Pb-free solder

5.1 Objective

The objective of this project is to provide thermal fatigue model in calcePWA and calceFAST for packages with ternary Pb-free solder (Sn3.9Ag0.6Cu).

5.2 Guidelines for Using Thermal Fatigue Models

There are many different thermal fatigue models available. By all means, FEM is the most thorough model since it considers complex geometry, complex temperature cycles and complex interconnect geometry. But it requires modeling expertise and it takes quite a time. The MDRR/NFEM model trades off the complex interconnect geometry but by doing that, we can reduce process time. This model still evaluates specific joint detail and considers rather complex temperature cycle[21]. The 2nd order model is simpler than MDRR/NFEM model. This model trades off different temperature profiles. The simplest, therefore fastest model is 1st order model which relates shear strain caused by thermal mismatch to cycles failure. The more complicated the model is, the more time it requires to process. For that reason, the 1st order model is often a proper choice when a model is used for design comparisons, complete CCA assessment and assembly level design tradeoffs.

5.3 Background

CalcePWA and calceFAST have implemented the 1st order thermal fatigue model. The 1st order thermal fatigue model is based on Manson-Coffin damage model. It relates inelastic strain range to cycles to failure with material constants. [22, 23]

$$N_f = \frac{1}{2}\left(\frac{\Delta\gamma_p}{2\varepsilon_f}\right)^{\frac{1}{c}} \tag{28}$$

$\Delta\gamma_p$: inelastic strain range

N_f: cycles to failure

ε_f, c: material constants

Inelastic strain range ($\Delta\gamma_p$) is a function of package type, geometry, dimension, material properties and load profile. For the simple package shown in Figure 42, the inelastic strain range is calculated as follows.

$$\Delta\gamma_p = \frac{L_a}{2h}(\Delta\alpha\Delta T) \tag{29}$$

$\Delta\alpha$: mismatch of coefficients of thermal expansion

ΔT: temperature difference

h: height of solder joint

L_a: span of solder balls

For eutectic solder, the material constants for the 1st order thermal fatigue model are known as follows [23].

$\varepsilon_f = 0.325$

$$c = -0.442 - 0.0006T_{sj} + 0.0174\ln\left(1 + \frac{360}{t_D}\right) \quad \textbf{(30)}$$

T_{sj}: mean cyclic temperature in degree C,

T_D: dwell in minutes at the maximum temperature.

To extend applicability of the 1st order thermal fatigue model in a domain of the ternary lead-free solder (Sn3.9Ag0.6Cu), the value ε_f and c are to be determined.

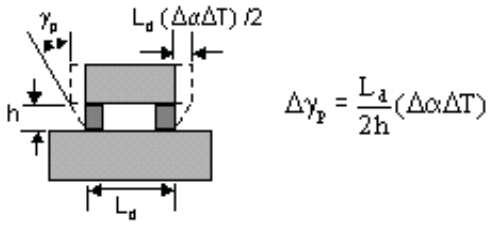

$$\Delta\gamma_p = \frac{L_d}{2h}(\Delta\alpha\Delta T)$$

$$N_f = \frac{1}{2}\left(\frac{\Delta\gamma_p}{2\varepsilon_f}\right)^{\frac{1}{c}}$$

- N_f: mean number of cycles to failure
- $\Delta\gamma_p$: inelastic strain range, g (package type, geometry, dimension, material property, load profile)
- ε_f = material constant, fatigue ductility coefficient
- c = material constant, fatigue ductility exponent, h (load profile)

For eutectic solder,

- $\varepsilon_f = 0.325$
- $c = -0.442 - 0.0006T_{sj} + 0.0174\ln\left(1 + \frac{360}{t_D}\right)$

- T_{sj}: mean cyclic temp. (°C)
- t_D: dwell in minutes at the max. temp.

Figure 42 1st order Thermal Fatigue Model

5.4 Approach

The material constants, ε_f and c for the ternary solder Sn3.9Ag0.6Cu are obtained from the procedure shown in Figure 43. The detail description of the assemblies and the thermal cycling profile were used as input parameters for calcePWA or calceFAST, and the inelastic strain range ($\Delta\gamma_p$) was calculated. The values of material constants (ε_f, c) were obtained from the relationship between the inelastic strain range ($\Delta\gamma_p$) and the cycles to failure (N_f).

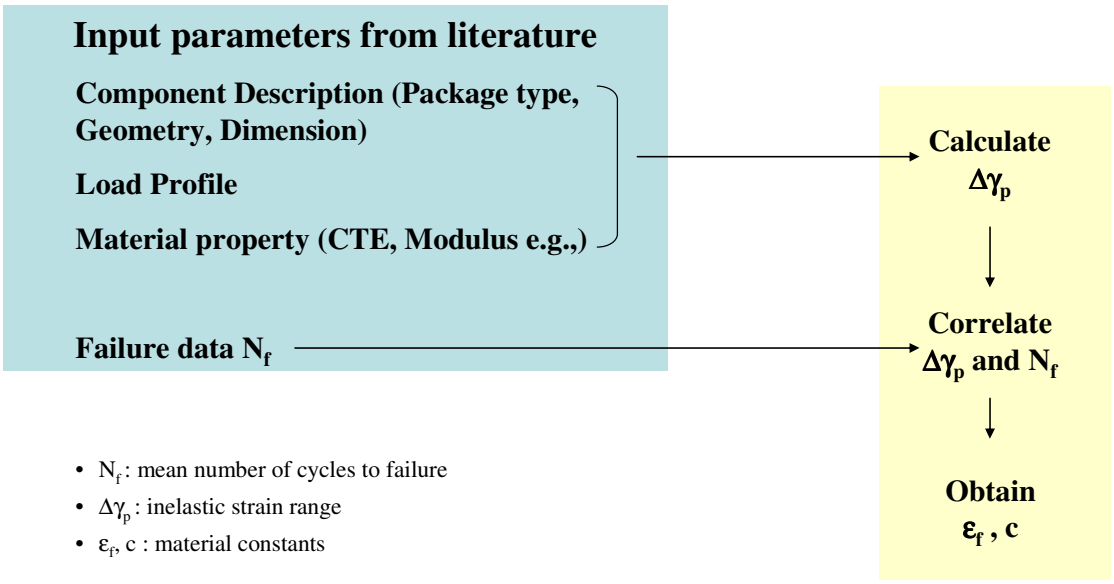

Figure 43 Approach

5.5 Failure data in literature

Figure 44 shows example of failure data found in the literature[24]. The package was a fleXBGA (12 mm × 12 mm): ball size of 30mils, pitch of 0.8 mm and die size of 6.4 mm × 6.4 mm, substrate material of tape. The chart shows cycles to

failure for 3 different solder materials under a thermal cycle of 0°C to 100°C with 10 minute ramp and 5 minute dwell time.

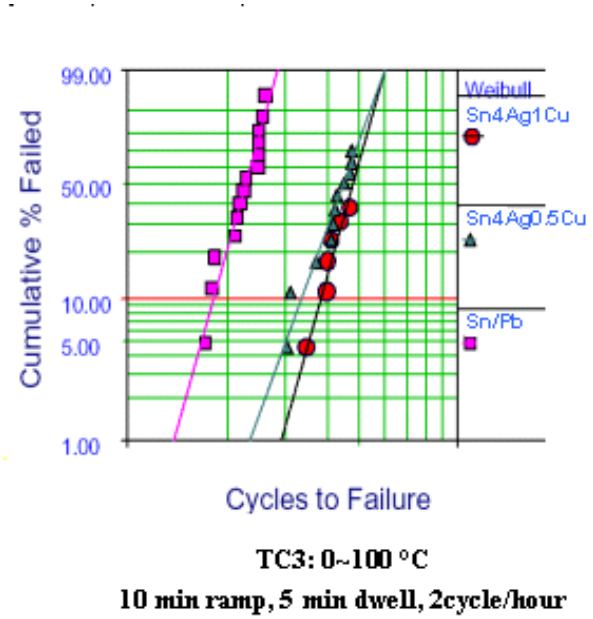

Figure 44 Failure Data of fleXBGA [24]

5.6 Variation in failure data

Table 6 summarizes the failure data available in the literature[25-36]. Tested packages include PBGA, CSP type packages, Chip Resistor, Flip Chip and LCCC. Testing temperatures vary from 0°C to 100°C to –55°C to 160°C. Some are thermal shock tests where dual chamber or tri-zone chamber was used.

Another variation is the actual composition of the ternary solder. The amount of variation is above the manufacturing specification (0.2%) as can be seen in Figure 45. The package was a fleXBGA (12 mm × 12 mm): ball size of 30mils, pitch of 0.8 mm and die size of 6.4 mm × 6.4 mm, substrate material of tape. The chart shows

cycles to failure for 3 different solder materials under a thermal cycle of -40°C to 125°C with 15 minute ramp and dwell, 1 cycle/hour.

For some cases, even mixed technology was used where a Pb-free paste was used with Sn-Pb balls as seen in Figure 46. Both cases, the packages were PBGA. The left side is about PBGA (15 mm × 15 mm): I/O 196, ball pitch of 1.0 mm and die size of 330mil × 330mil. The left chart shows cycles to failure for two different solder materials under a thermal cycle of -40°C to 125°C with 11 minute ramp and 15 minute dwell at maximum temperature and 15 minute dwell at minimum temperature, 60min/cycle. The right side is about PBGA (35 mm × 35 mm): I/O 388, ball pitch of 1.27 mm and die size of 330mil × 330mil. The right chart shows cycles to failure for two different solder materials under a thermal cycle of 0°C to 100°C with 10 minute ramp and 10 minute dwell at maximum temperature and 10 minute dwell at minimum temperature, 40min/cycle.

Board surface finish was another important issue that caused variation as can be seen in Figure 47. The same Chip resistors under the same loading exhibit different lifetime depending on the surface finish.

Table 6 Failure data available in literature

Author	Composition	Package Type	Load Profile
Roubaud	Sn4Ag0.5Cu	PBGA, M2CSP	0~100 °C -40~125 °C
Syed	Sn4Ag0.5Cu Sn3.4Ag0.7Cu	PBGA, fleXBGA Chip Array	-40~125 °C -55~125 °C 0~100 °C
Woodrow	Sn3.8Ag0.7Cu	Chip resistors	- 55~ 125 °C
Zhang	Sn3.8Ag0.7Cu	Flip Chip	0 ~ 100 °C
Woosley/Swan	Sn3.8Ag0.7Cu	PBGA Chip resistors	-40 ~ 125 °C - 55~ 125 °C
Primavera	Sn3.8Ag0.7Cu	PBGA	0 ~ 100 °C -40 ~ 125 °C
Raytheon	Sn4Ag0.5Cu	Tape Array □BGA	-40 ~ 125 °C
Dusek	Sn3.8Ag0.7Cu	Chip resistors	- 55~ 125 °C
Schubert et al.	Sn3.8Ag0.7Cu	Flip Chip Chip resistors	- 55~ 125 °C - 55~ 150 °C
Frear et al.	Sn3.8Ag0.7Cu	Flip Chip	0 ~ 100 °C -40 ~ 125 °C
NCMS	Sn4Ag0.5Cu	LCCC Chip resistors PBGA FleXBGA	-55 ~ 160 °C -40 ~ 125 °C 0 ~ 100 °C

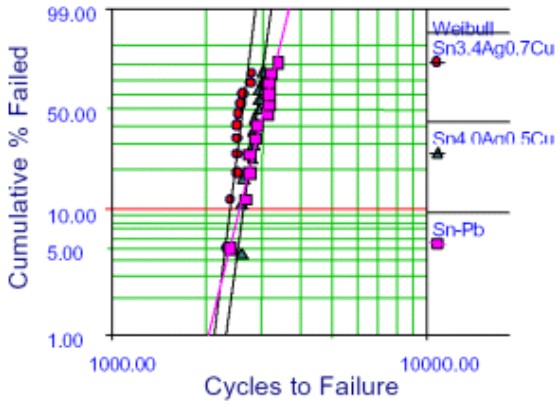

Figure 45 Various Ternary Solder Compositions in the Published Data [24]

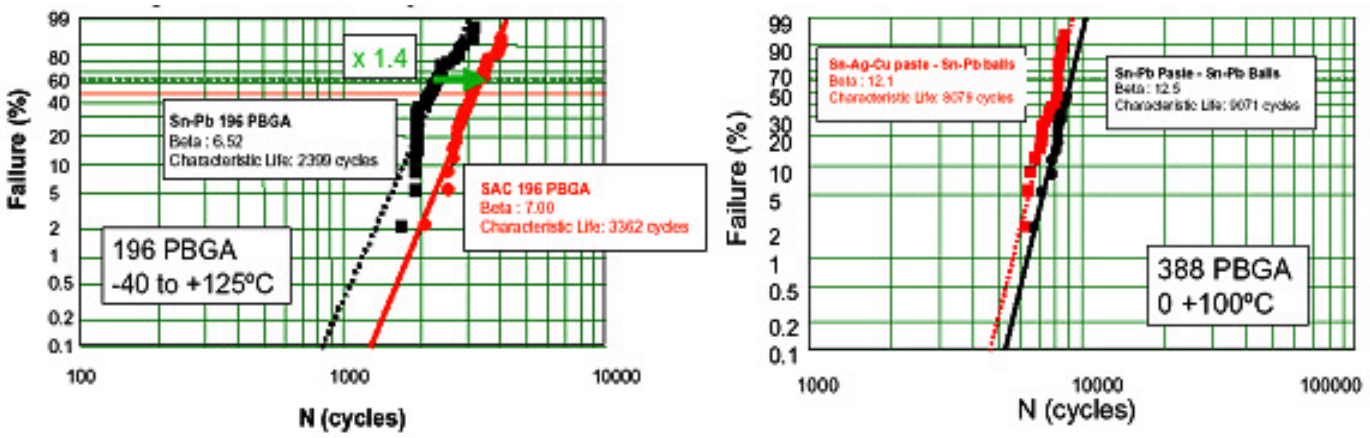

Figure 46 Mixed Technology in the Published Data [25]

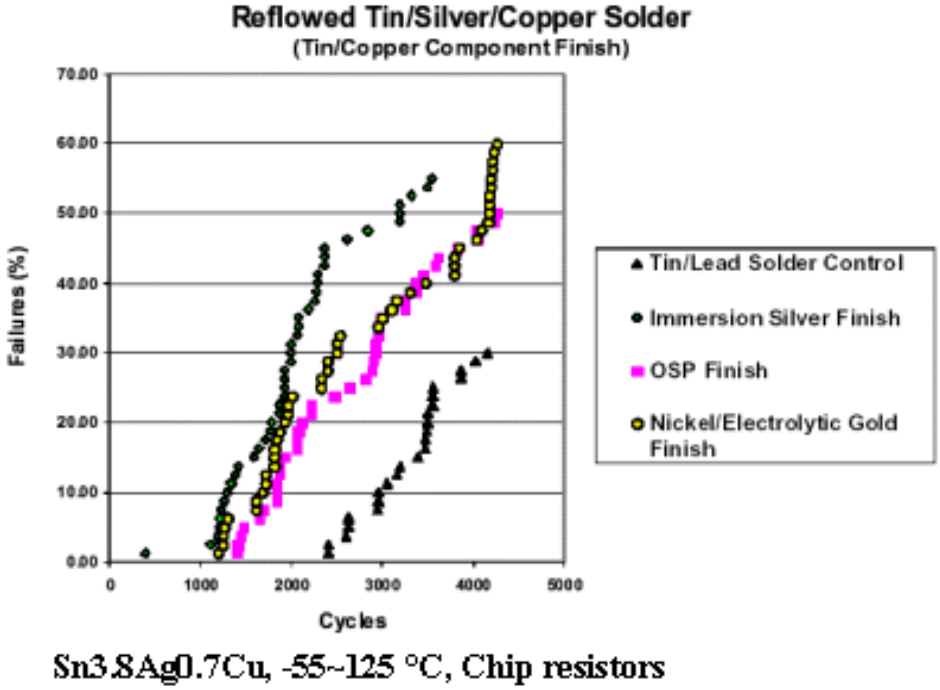

Figure 47 Effect of Surface Finish [37]

5.7 Summary from the Published Data

The information in the literature can be summarized as:

– It would be reasonably safe to assume that Pb-free solders are more robust than standard eutectic solder except for some leadless type packages.

– Other issues including board finish, intermetallics species and formation etc. can become more critical than intrinsic material durability.

– Acceleration factors are higher for Pb-free solders.

5.8 Determination of Material Constants

For each thermal cycle test, inelastic strain was calculated using calcePWA or calceFAST. As illustrated in Figure 48, the input parameters are package type, geometry, dimension and material used, load profile and material properties such as CTE and modulus. For the missing parameters, the values were assumed to be nominal ones[38].

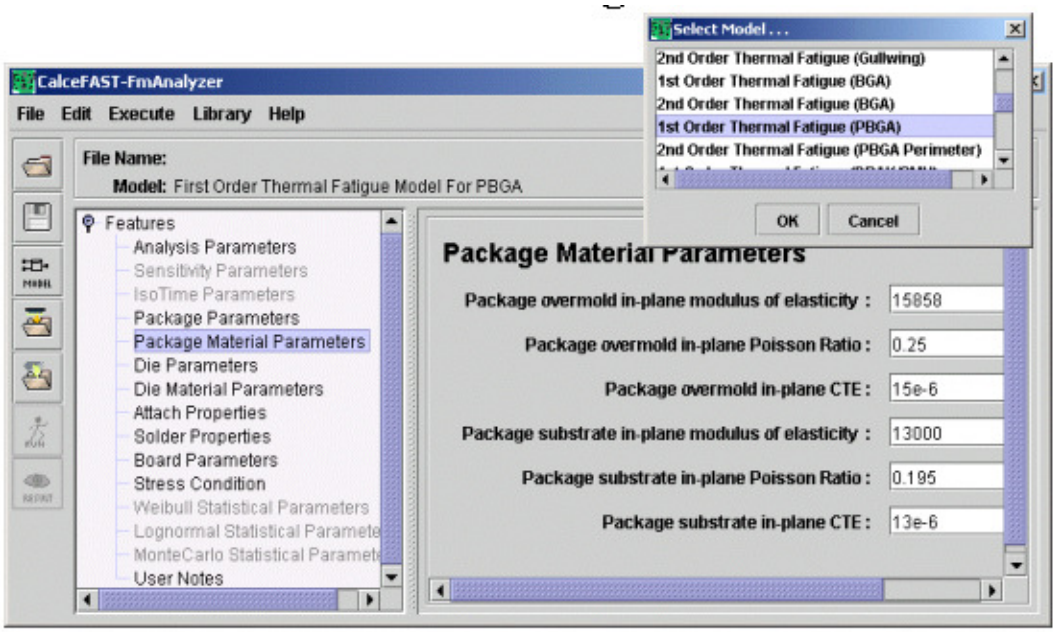

Figure 48 Strain Calculation using calceFAST

By correlating the inelastic strain ranges ($\Delta\gamma_p$) and the cycles to failure data (N_f), the material constants ε_f and c were obtained. ε_f is a simple constant and c is expected to be a function of dwell time (t_D) and time averaged temperature (Tsj).

The ternary solder data available in the literature did not exhibit much variation in dwell time (t_D) and time averaged temperature (Tsj) as shown in Table 7. The exponent c was then assumed to be a constant.

Taking log on both sides of equation (28), it becomes

$$\log \Delta\gamma_p = c \log\left(2N_f\right) + \log\left(2\varepsilon_f\right) \quad \textbf{(31)}$$

$\Delta\gamma_p$: inelastic strain range

N_f: cycles to failure

ε_f, c: material constants

The relationship between the inelastic strain range ($\Delta\gamma_p$) and twice of the cycles to failure ($2N_f$) for each thermal cycle test is plotted in Figure 49. It clearly shows a linear relationship. The constants for the relationship were obtained by least square fitting. The constant c was obtained from the slope, and the value of ε_f was obtained from the y-axis intercept. The results are written as

$$\log \Delta\gamma_p = -0.285 \log\left(2N_f\right) + \log 0.26 \quad \textbf{(32)}$$

$c = -0.285$

$\varepsilon_f = 0.13$

Table 7 Dwell time and Mean temperature for each case

Package Type	Temperature range (°C)	Time Averaged Temperature in °C (T_{sj})	Dwell Time in minutes (t_D)	Reference
fleXBGA	-40 to 125	42.5	15	[24]
	-55 to 125	35	13	[24]
	0 to 100	50	5	[24]
	-55 to 125	41.2	15	[31]
Flip Chip	0 to 100	N/A	N/A	[28]
ChipArray	-40 to 125	42.5	15	[24]
2512 Chip Resistor	-40 to 125	35	5	[29]
	-55 to 125	50	5	[29]
	0 to 100	42.5	15	[29]
	-55 to 125	35	5	[32]
1206 Chip Resistor	-55 to 125	35	15	[27]
	-40 to 150	55	12	[35]
M2CSP	0 to 100	50	10	[25]
	-40 to 125	42.5	15	[25]
PBGA	-40 to 125	42.5	15	[24]
	-40 to 125	425	15	[25]
	-40 to 125	425	15	[39]
	-55 to 125	35	5	[39]
	0 to 100	50	5	[30]
	-40 to 125	42.6	14	[30]
	-55 to 125	41.2	15	[27]
	-40 to 125	42.5	15	[29]
	-55 to 125	35	5	[29]

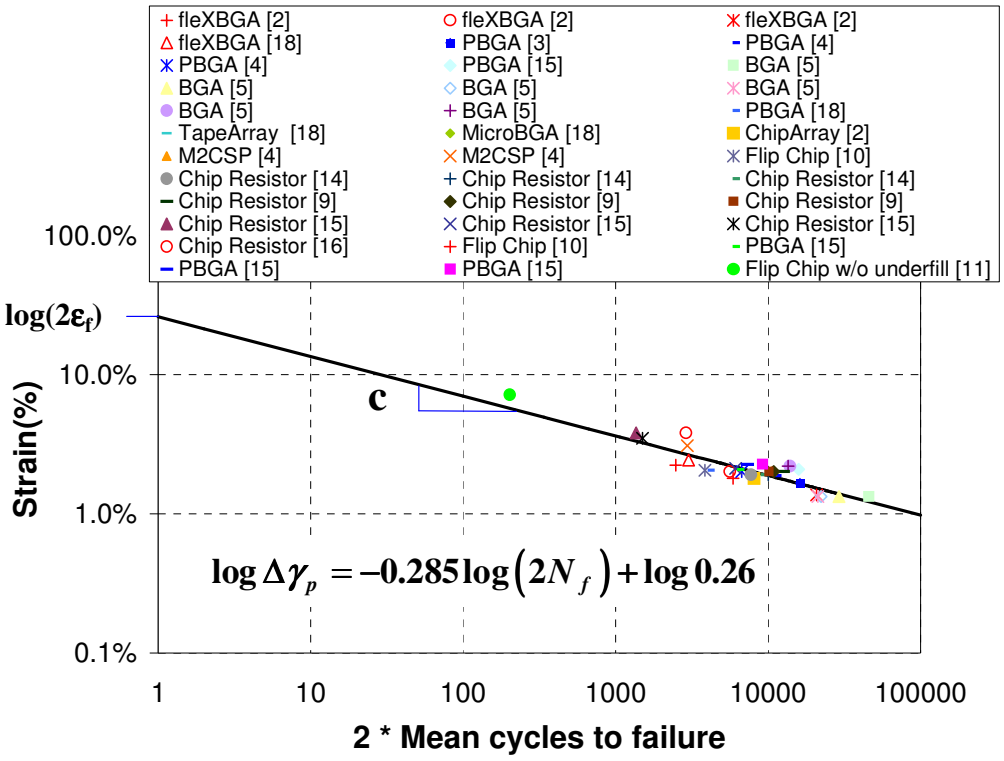

Figure 49 Correlation between Inelastic Strain Range and Cycles to Failure

Chapter 6: Conclusions and Future Studies

6.1 Conclusions

An advanced micro shear test with modified single lap specimen configuration was proposed for determination of the constitutive properties of solder alloys.

With the aid of the extension unit, shear deformation is measured without compensating machine and grip compliance, which enhances measurement accuracy substantially.

The specimen configuration includes geometrical constraints at the solder and substrate interfaces in most electronic assemblies. Consequently, the results represent pseudo-continuum properties that account for the constraints at the interface. These properties are more realistic for continuum mechanics based stress studies.

Sn3.5Ag solder is one of the commonly recommended Pb-free solder candidate. Constitutive behavior of Sn3.5Ag binary solder was characterized by adopting the proposed test scheme. Isothermal constant strain rate tests were performed at three different temperatures and seven different strain rates to measure temperature and strain rate dependent behavior of Sn3.5Ag. The temperatures are 25ºC, 75 ºC, 125 ºC and the constant strain rates are $1\times10^{-1}s^{-1}$, $1\times10^{-2}s^{-1}$, $1\times10^{-3}s^{-1}$, $1\times10^{-4}s^{-1}$, $1\times10^{-5}s^{-1}$, $1\times10^{-6}s^{-1}$ $1\times10^{-7}s^{-1}$.

To describe the temperature and strain rate dependent behavior of Sn3.5Ag, two different approaches were taken. For partitioned approach, material parameters for

elastic, time-independent plastic and creep model were obtained by curve fitting. And for unified approach, material specific constants were obtained for Anand model with nonlinear least square fitting method.

Finally, 1st order thermal fatigue model was calibrated for ternary lead-free solder (Sn3.9Ag0.6Cu). All the failure data available from literature at the time of research were visited. The failure data are from many different packages including PBGA, fleXBGA, chip resistors and flip chip and the loading temperature profile covers from -55 ºC to 160 ºC. Inelastic strain range ($\Delta\gamma_p$) was calculated using CalcePWA and CalceFAST based on the information available in literature which includes package type, geometry, dimension and material used, load profile and material properties such as CTE and modulus. The material constants (ε_f, c) were obtained By correlating the calculated inelastic strain range ($\Delta\gamma_p$) and the cycles to failure (N_f).

Appendix A. Matlab codes used to obtain Anand constants

The followings are the codes created to obtain Anand constants.

$$\sigma^* = \frac{\hat{s}}{\xi}\left(\frac{\dot{\varepsilon}_p}{A}e^{Q/RT}\right)^n \sinh^{-1}\left[\left(\frac{\dot{\varepsilon}_p}{A}e^{Q/RT}\right)^m\right]$$

The 'anand_nonlin.m' and 'myfun_real.m' code are to obtain material constants, Q/R, A, $\hat{s}/\xi$, m and n in the above equation.

It can be determined by a nonlinear least square fitting of $\dot{\varepsilon}_p$ ~ σ^* data from the experimental results. 'lsqnonlin' command in Matlab was used. The manual for 'lsqnonlin' can be downloaded on line. It is in the Optimization ToolBox manual which locates at

http://www.mathworks.com/access/helpdesk/help/pdf_doc/optim/optim_tb.pdf

```
**************************************************************************
********************** anand_nonlin.m ****************************
**************************************************************************
% This is the main code to obtain Q/R, A, ŝ/ξ, m and n
x0 = [10 1e4 1000 0.01 0.1]; % initial value

%x0(1)=s hat over xi
%x0(2)=A
%x0(3)=Q/R
%x0(4)=n
%x0(5)=m
options=optimset('display','iter','MaxFunEvals',1000000000,'MaxIter'
,10000000)
[x,resnorm] = lsqnonlin('myfun_real',x0,0,inf,options)

%[x,resnorm] = lsqnonlin(...) returns the value of the squared 2-
norm of the residual at x: sum(fun(x).^2).
%lsqnonlin(fun,x0,lb,ub,options) minimizes with the optimization
parameters specified in the structure options. Pass empty matrices
for lb an ub if no bounds exist.

**************************************************************************
************************ myfun_real.m ****************************
```

```
**********************************************************************
function F = myfun_real(x0)
%si=saturated stress obtained from experiments
si=[13.37
18.84
12.3
10.61
6.91
6.408
5.38
21.7
19
16
14.01
1.29E+01
1.74E+01
22.44
27.53247
28.8875
35.55
38.33
46.3];
si=si*sqrt(3); %equivalent stress
%ep= strain rate from experiments conditions
ep=[1.00E-03
1.00E-02
1.65E-04
2.54E-05
3.56E-06
1.00E-06
1.00E-07
0.001
1.00E-04
1.00E-05
0.000001
2.47E-08
1.96E-07
2.89E-06
1.00E-05
0.0001
0.001
1.00E-02
1.00E-01];
ep=ep/sqrt(3); %equivalent strain
%T=temperature from experiments conditions
T=[398 398 398 398 398 398 398 348 348 348 348 298 298 298 298 298
298 298 298];
T=T';
k=1:19; %19=number of data set
%x0(1)=s hat over xi
%x0(2)=A
%x0(3)=Q/R
%x0(4)=n
%x0(5)=m
%F=stress calculated from flow equation - stress obtained
```

```
F =
x0(1).*(ep(k)./x0(2).*exp(x0(3)./T(k))).^x0(4).*asinh((ep(k)./x0(2).
*exp(x0(3)./T(k))).^x0(5))-si(k);
```

```
**************************************************************************
************************ anand_plot.m ****************************
**************************************************************************
% This code is to plot strain rate vs. stress w/ the constants
obtained from nonlinear least square fitting.
% assign values as obtained from nonlinear square fitting
sok=0.00033098123207e+004;
A=2.24555734198725e+004;
QoR=1.21090551777079e+004;
n=0.00000271024010e+004;
m=0.00003843662027e+004;
% log scale x-axis set min. max.
logepdot=(-9:1:0);
epdot=10.^(logepdot);
% 3 plots for each temperature
T1=298;
T2=348;
T3=398;
% calculating stress from flow equation
sigstart1=sok.*(epdot./A.*exp(QoR./T1)).^n.*asinh((epdot./A.*exp(QoR
./T1)).^m);
sigstart2=sok.*(epdot./A.*exp(QoR./T2)).^n.*asinh((epdot./A.*exp(QoR
./T2)).^m);
sigstart3=sok.*(epdot./A.*exp(QoR./T3)).^n.*asinh((epdot./A.*exp(QoR
./T3)).^m);
% convert stress values to shear stress value
shearsig1=sigstart1/sqrt(3);
shearsig2=sigstart2/sqrt(3);
shearsig3=sigstart3/sqrt(3);
% convert strain rate to shear strain value
epdot=epdot*sqrt(3);
% plot the graph
plot(log10(shearsig1),log10(epdot))
hold % to draw 3 lines in one plot
plot(log10(shearsig2),log10(epdot))
plot(log10(shearsig3),log10(epdot))
k=18;
c=1./k.*asinh((epdot./A.*exp(QoR./T1)).^m)
```

```
**************************************************************************
**************************************************************************
```

The next codes are to obtain 3 other constants.

$$\sigma = \sigma^* - \left[\left(\sigma^* - cs_0 \right)^{(1-a)} + (a-1) \left\{ \left(ch_0 \right) \left(\sigma^* \right)^{-a} \right\} \varepsilon_p \right]^{\frac{1}{1-a}} \qquad (33)$$

Three material constants h_0, a, and s_0 of Eq. 19 can be determined by applying a nonlinear least square fitting of $\varepsilon_p \sim \sigma$ curves near the transient region. The set of constants were obtained for each constant strain rate test and they were averaged.

```
**************************************************************************
************************  evol_nonlin.m  ************************
**************************************************************************
%This is main code to obtain h0, a, and s0

x0 = [45.48 1.19 7933.5]; %initial value of So, a, ho
options=optimset('display','iter','MaxFunEvals',1000000000,'MaxIter'
,10000000)
[x,resnorm] = lsqnonlin('myfun_evol_test1',x0,0,inf,options)

**************************************************************************
********************** myfun_evol_test1.m ************************
**************************************************************************
%This code requires set of shear plastic strain and shear stress
data in transient region from the experiment
function F = myfun_evol_test1(x0)
%ps: shear plastic strain data from experiment test1
ps=[**
**
**
**];
%ss: shear stress data from test1
ss=[**
**
**
**];
ps=ps/sqrt(3);
ss=ss*sqrt(3);
k=1:268; % number of strain vs stress data set
sigstar=22.44*sqrt(3); %saturated stress obtained from test1
ep=2.89e-6/sqrt(3);
T=298; % temperature condition from test1
ksi=18; %ξ value obtained from previous nonlinear least square curve fitting
aa=22450; %A value obtained from previous nonlinear least square curve fitting
QoR=12406; %Q/R value obtained from previous nonlinear least square curve fitting
m=0.4988; %m value obtained from previous nonlinear least square curve fitting
c=1./ksi.*asinh((ep./aa.*exp(QoR./T)).^m);
F=sigstar-((sigstar-c.*x0(1)).^(1-x0(2))+(x0(2)-
1).*((c.*x0(3)).*sigstar.^(-x0(2))).*ps(k)).^(1./(1-x0(2)))-ss(k);


**************************************************************************
**************************************************************************
```

Bibliography

1. Darveaux, R., *Solder joint fatigue life modeling*. Design and Reliability of solders and solder interconnections. 1997. 213-218.
2. Darveaux, R. and K. Banerji, *Constitutive Relations for Tin-based Solder Joints.* IEEE Transaction on Components, Hybrids and Manufacturing Technology, 1992. **15**(6): p. 1013-1024.
3. Ye, H., M. Lin, and C. Basaran, *Failure Modes and FEM analysis of power electronic packaging.* Finite Elements in Analysis and Design, 2002. **38**.
4. Wang, G.Z., et al., *Applying Anand Model to Represent the Viscoplastic Deformation Behavior of Solder Alloys.* Journal of Electronic Packaging, 2001. **123**: p. 247-253.
5. Darveaux, R., et al., *Reliability of plastic ball grid array technology*. Ball grid array technology. 1995. pp. 379-442.
6. Pollack, D., *Validation of constitutive properties of Anand model as applied to thermo-mechanicla deformation analysis of eutectic solder*, in *Mechanical Engineering*. 2003, University of Maryland: College Park.
7. Haswell, P., *Durability Assessment and Microstructural Observations of Selected Solder Alloys*, in *Mechanical Engineering*. 2001, University of Maryland: College Park.
8. Iosipesc, N., *New Accurate Procedure for Single Shear Testing of Metals.* Journal of Materials, 1967. **2**(3): p. 537-&.
9. Reinikainen, T. and W. Ren. *An Optimized Shear Test Sample for Assessing Solder Deformation Properties*. in *EuroSimE*. 2001. Paris.
10. Reinikainen, T., et al., *A finite-element and experimental analysis of stress distribution in various shear tests for solder joints.* Journal of Electronic Packaging, 1998. **120**(1): p. 106-113.
11. Zhang, Q., *Isothermal Mechanical and Thermomechanical Durability Characterization of Selected Pb-free Solders*, in *Mechanical Engineering*. 2004, University of Maryland: College Park.
12. *Standard Practice for Verification of Specimen Alignment under Tensile Loading*, ASME Standard. p. E1012-99.
13. Anand, L., *Constitutive Equations for the Rate-Dependent Deformation of Metals at Elevated Temperatures.* Journal of Electronic Materials and Technology, Transactions of the ASME, 1982. **104**(1): p. 12-17.
14. Skipor, A.F., S.V. Harren, and J. Botsis, *On the constitutive response of 63/37 Sn/Pb eutectic solder.* Journal of Engineering Materials and Technology-Transactions of the Asme, 1996. **118**(1): p. 1-11.
15. Mavoori, H., et al., *Creep, Stress Relaxation, and Plastic Deformation in Sn-Ag and Sn-Zn Eutectic Solders.* Journal of Electronic Materials, 1999. **26**(7): p. 783-790.
16. Chan, K.S. and e. al, *A survey of Unified Constitutive Theories*, in *NASA report*. 1984.

17. Wilde, J., et al., *Rate Dependent Constitutive Relations Based on Anand Model for 92.5Pb5Sn2.5Ag Solder.* IEEE Transaction on Advanced Packaging, 2000. **23**(3): p. 408-414.
18. Cheng, Z.N., et al., *Viscoplastic Anand Model for Solder Alloys and its Application.* Soldering and Surface Mount Technology, 2000. **12**(2): p. 31-36.
19. Darveaux, R. *Effect of Simulation Methodology on Solder Joint Crack Growth Correlation*. in *IEEE Electronic Component and Technology Conference*. 2000.
20. Amagai, M., et al., *Mechanical Characterization of Sn-Ag-based Lead-free Solders.* Microelectronics Reliability, 2002. **42**: p. 951-966.
21. Ling, S. and A. Dasgupta, *A nonlinear multi-domain thermomechanical stress analysis method for surface mount solder joints.2. Viscoplastic analysis.* Journal of Electronic Packaging, 1997. **119**(3): p. 177-182.
22. Osterman, M. *Explanation of the 1st Order Thermal Fatigue Model for Solder Interconnects in Leaded (J-Lead and Gullwing) and Leadless Packages*. in *calcePWA Software Documentation*.
23. Engelmaier, W., *Fatigue Life of Leadless Chip Carrier Solder Joints During Power Cycling.* Components, Hybrids, and Manufacturing Technology, IEEE Transactions on [see also IEEE Trans. on Components, Packaging, and Manufacturing Technology, Part A, B, C], 1983. **6**(3): p. 232.
24. Syed, A. *Reliability and Au embrittlement of lead free solders for BGA applications*. in *IEEE International Symposium on Advanced Packaging Materials Processes, Properties and Interfaces*. 2001. Piscataway, NJ, USA.
25. Roubaud, P., et al. *Thermal fatigue resistance of Pb-free second level interconnect*. in *SMTA International. Proceedings of the Technical Program*. 2001. Edina, MN, USA: Surface Mount Technol. Assoc.
26. Syed, A. *Reliability of Lead-Free Solder Connections for Area-Array Packages*. in *IPC SMEMA Council APEX*. 2001.
27. Woodrow, A. *Reliability and Leachate Testing of Lead-Free Solder Joints*. in *International Conference on Lead-Free Components and Assemblies*. 2002. San Jose, CA.
28. Zhang, C., J. Lin, and L. Li. *Thermal fatigue properties of lead-free solders on Cu and NiP under bump metallurgies*. in *IEEE 51st Electronic Components and Technology Conference*. 2001. Piscataway, NJ, USA.
29. Swan, G., et al. *Development of Lead-Free Peripheral Leaded and PBGA Components to Meet MSL3 at 260°C Peak Reflow Profile*. in *IPC APEX*. 2001. San Diego, CA.
30. Meilunas, M., A. Primavera, and S. Dunford. *Reliability and Failure Analysis of Lead-Free Solder Joints*. in *IPC Annual Meeting*. 2002. New Orleans, USA.
31. *Thermal cycle fatigue data from Raytheon*.
32. Dusek, M., J. Nottay, and C. Hunt. *Compatibility of Lead-Free Alloys with Current PCB Materials*. in *International Conference on Advanced Packaging and Systems*. 2002. Reno, NV.

33. Schubert, A., et al. *Lead-free Solder Interconnects: Characterization, Testing and Reliability*. in *3rd. Int. Conf. On Benefiting from Thermal and Mechanical Simulation in (Micro-) Electronics, EuroSIME2002*. 2002.
34. Schubert, A., et al., *Lead-free Flip-Chip Interconnects-Materials Mechanics and Reliability Issues.* Micromaterials and Nanomaterials, 2002. **1**: p. 13-25.
35. Schubert, A., et al. *Reliability assessment of flip-chip assemblies with lead-free solder joints*. in *IEEE 52nd Electronic Components and Technology Conference*. 2002. Piscataway, NJ.
36. Frear, D.R., et al., *Pb-free solders for flip-chip interconnects.* JOM, 2001. **53**(6): p. 28-32, 38.
37. *Lead Elimination from PWA Assemblies*, in *2002 Boeing A&M environmental technotes*.
38. Siewert, T., et al., *Database for Solder Properties with Emphasis on New Lead-free Solders*, N.a.C.S.o. Mines, Editor.
39. Yushi, M., et al. *Development of Environmentally Preferred Plastic Ball Grid Array, PBGA, Components*. in *2nd International Symposium on Environmentally Conscious Design and Inverse Manufacturing, EcoDesign 2001*. 2001.